Ana Lúcia Moreira Pinto

Licenciada em Bioquímica

Light Harvesting in Solar Cells using Natural Pigments from Red Fruits Adsorbed to Mesoporous TiO_2

Dissertação para obtenção do Grau de Mestre em
Biotecnologia

Orientador: Dr. César A. T. Laia, Investigador Auxiliar, Faculdade de Ciências e Tecnologia – Universidade Nova de Lisboa

Co-orientador: Dr. A. Jorge Parola, Professor Associado, Faculdade de Ciências e Tecnologia – Universidade Nova de Lisboa

Júri:

Presidente: Dr. Pedro Miguel Ribeiro Viana Baptista, Professor Associado com Agregação, Faculdade de Ciências e Tecnologia – Universidade Nova de Lisboa

Arguente: Dra. Suzana Maria de Andrade Sousa Paiva, Colaboradora Docente, Instituto Superior Técnico – Universidade de Lisboa

FACULDADE DE CIÊNCIAS E TECNOLOGIA
UNIVERSIDADE NOVA DE LISBOA

Novembro, 2015

Ana Lúcia Moreira Pinto

Licenciada em Bioquímica

Light Harvesting in Solar Cells using Natural Pigments from Red Fruits Adsorbed to Mesoporous TiO_2

Dissertação para obtenção do Grau de Mestre em
Biotecnologia

Orientador: Dr. César A. T. Laia, Investigador Auxiliar, Faculdade de Ciências e Tecnologia – Universidade Nova de Lisboa

Co-orientador: Dr. A. Jorge Parola, Professor Associado, Faculdade de Ciências e Tecnologia – Universidade Nova de Lisboa

Júri:

Presidente: Dr. Pedro Miguel Ribeiro Viana Baptista, Professor Associado com Agregação, Faculdade de Ciências e Tecnologia – Universidade Nova de Lisboa

Arguente: Dra. Suzana Maria de Andrade Sousa Paiva, Colaboradora Docente, Instituto Superior Técnico – Universidade de Lisboa

FACULDADE DE CIÊNCIAS E TECNOLOGIA
UNIVERSIDADE NOVA DE LISBOA

Novembro, 2015

Light Harvesting in Solar Cells using Natural Pigments from Red Fruits Adsorbed to Mesoporous TiO_2

Acknowledgements

First, I would like to express my sincere gratitude to the Photochemistry Laboratory from the Chemistry Department from the Faculdade de Ciências e Tecnologia – UNL for having me and supporting my master thesis. I would like to acknowledge Prof. Dr. César Laia for thinking of me to develop this work, for teaching me, for helping me develop the necessary tools to grow professionally and for, sometimes, believing in me even more than myself. I would also like to thank Profs. Dr. Jorge Parola and Dr. João Lima for being so available to answer my questions and for advising, helping and teaching me.

I would also like to acknowledge Isabel Nogueira, from MicroLab - IST, Nuno Costa from the Analysis Laboratory of REQUIMTE – FCT/UNL, Dr. Ana Pimentel and Alexandra Gonçalves from CENIMAT – FCT/UNL and Dr. Luísa Andrade and Dr. Cláudia Costa from LEPABE - Faculty of Engineering, University of Porto for their help and contribution for this work.

I would like to thank all my laboratory colleagues, especially Andreia Ruivo, Luís Cabrita, Nuno Basílio, Sandra Gago and Tiago Moreira for the help and the patience for teaching me throughout this work. To all my colleagues, thank you so much for the support, the advices and, most of all, thank you all for the friendship. I am very happy and thankful for everything I have learnt from you this past year.

I would also like to thank my colleagues, especially Tiago Mestre and Bruno Pedras, for being a part of my professional and personal life for the past five years. Some of you are more than work colleagues, you are my friends with whom I shared memorable moments. We saw and helped each other grow and fight to be better professionals and better people. I must thank you all for being a part of this.

Finally, I want to thank my family and friends. To my mother, my father, my two sisters and my godmother, thank you for the support, the education, the comprehension, the love and for teaching me to fight for what I want. I would like to thank Fernando Poças for being like an older brother, always present and always so loyal. Finally, I want to thank António Barreto for, basically, everything. You were all essential in helping me pull through this stage of my life.

This work was supported by the European project NMP4-SL-2012-310651 under FP7-NMP-2012-SMALL-6.

Table of Contents

Abstract

Nature has developed strategies to present us with a wide variety of colours, from the green of leaves to the bright colours seen in flowers. Anthocyanins are between these natural pigments that are responsible for the great diversity of colours seen in flowers and fruits. Anthocyanins have been used to sensitize titanium dioxide (TiO_2) in Dye-Sensitized Solar Cells (DSSCs). DSSCs have become one of the most popular research topic in photovoltaic cells due to their low production costs when compared to other alternatives. DSSCs are inspired in what happens in nature during photosynthesis. A primary charge separation is achieved by means of a photoexcited dye capable of performing the electron injection into the conduction band of a wide band-gap semiconductor, usually TiO_2.

With this work we aimed to synthesize a novel mesoporous TiO_2 structure as the semiconductor in order to increase the dye loading. We used natural occurring dyes such as anthocyanins and their synthetic flavylium relatives, as an alternative to the widely used metal complexes of Ru(II) which are expensive and are environmentally unsafe. This offers not only the chance to use safer dyes for DSSCs, but also to take profit of waste biological products, such as wine and olive oil production residues that are heavily loaded with anthocyanin dyes. We also performed a photodegradation study using TiO_2 as the catalyst to degrade dye contaminants, such as those from the wine production waste, by photo-irradiation of the system in the visible region of the light spectrum.

We were able to succeed in the synthesis of mesoporous TiO_2 both powder and thin film, with a high capacity to load a large amount of dye. We proved the concept of photodegradation using TiO_2 as catalyst. And finally, we show that wine production waste is a possible dye source to DSSCs application.

Keywords: Natural Dyes, Photoinduced Reactions, Dye-Sensitized Solar Cells, Anthocyanins, Titanium Dioxide.

Resumo

A Natureza presenteia-nos com uma grande variedade de cores, desde o verde das folhas, às cores garridas das flores. As antocianinas são um dos corantes naturais responsáveis pela grande variedade de cores vista em flores e frutos. Estes pigmentos têm sido usados para sensitizar dióxido de titânio (TiO_2) em Células Solares Sensitizadas por Corantes (DSSCs, do inglês Dye-Sensitized Solar Cells). As DSSCs têm vindo a tornar-se um assunto muito atraente na área das células fotovoltaicas devido ao seu baixo custo de produção, quando comparado com outras alternativas. O funcionamento destas células é inspirado no processo fotossintético que ocorre na Natureza. Ou seja, o seu funcionamento baseia-se na injecção de um electrão na banda condutora de um semicondutor, normalmente o TiO_2, resultante da fotoexcitação do corante.

Um dos objectivos deste trabalho era o de sintetizar TiO_2 com uma estrutura mesoporosa por forma a aumentar a sua capacidade de adsorver corante. Utilizámos corantes naturais, tais como as antocianinas, bem como flavílios sintéticos, seus análogos, como uma alternativa aos corantes baseados em complexos de Ru(II) que, não só são caros, como prejudiciais para o meio ambiente. O uso de corantes naturais oferece não só a mais-valia de trabalhar com compostos 'amigos do ambiente', como também a possibilidade de reaproveitar resíduos biológicos provenientes da indústria, como por exemplo, resíduos das produções vinícula e de azeite, que estão fortemente carregadas de antocianinas naturais. Realizámos, ainda, um estudo de fotodegradação usando o TiO_2 como catalisador para degradar corantes, como o pigmento extraído dos resíduos da produção vinícula, através da irradiação do sistema com luz visível.

Fomos bem sucedidos na síntese de TiO_2 com estrutura mesoporosa e com uma grande capacidade para adsorção de compostos, tanto em pó como na forma de filme fino. Conseguimos provar o conceito de fotodegradação usando o TiO_2 como catalisador, sob irradiação com luz visível. E, ainda, provamos que é possível usar resíduos da produção vinícula como fonte de corantes naturais para aplicar em DSSCs.

Palavras-chave: Corantes naturais, Reacções foto-induzidas, Células Solares Sensitizadas por Corantes, Antocianinas, Dióxido de titânio.

Figures Index

Tables Index

Abbreviations List

Abs	Absorbance
ACF	Autocorrelation Function
a.u.	Arbitrary units
cm	Centimetres
D	Dye at ground state
D_h	Particle diameter
Diff	Diffusion coefficient
D*	Dye at excited state
DLS	Dynamic Light Scattering
DSC	Differential Scanning Calorimetry
DSSC	Dye-Sensitized Solar Cell
EDS	Energy-dispersive X-ray Spectroscopy
eV	Electron Volt
e^-	Electron
e^-_{cb}	Conduction band electron
FTO	Fluorine-doped tin oxide
HOMO	Highest Occupied Molecular Orbital
hν	Light
ITO	Indium-doped tin oxide
IUPAC	International Union of Pure and Applied Chemistry
JCPDS	Joint Committee on Powder Diffraction Standards
LUMO	Lowest Unoccupied Molecular Orbital
mA	milliAmpere
min	Minute
mM	milliMolar
mV	milliVolt
mW	milliWatt
M	Molar
nm	Nanometre
PV	Photovoltaic
rpm	Rotation per minute
s	Second

SEM	Scanning Electron Microscopy
t	Time
T	Temperature
TEM	Transmission Electron Microscopy
TEOS	Tetraethyl orthosylicate
TEOT	Titanium(IV) ethoxide
TGA	Thermogravimetric Analysis
UV	Ultra-violet
Vis	Visible
XRD	X-ray Diffraction
2θ	2-theta angle
η	Viscosity
λ	Wavelength
µm	Micrometre
µs	Microsecond
Ω	Ohm
τ	Relaxation time

1. Experimental Section

1.1. Materials

Ethanol absolute anhydrous (Carlo Erba, analytical grade), Hydrochloric Acid (Sigma-Aldrich, 37%, analytical grade), Titanium(IV) Tetraethoxide (Sigma-Aldrich, technical grade), Titanium Isopropoxide (Sigma-Aldrich, 97%), Pluronic P123 (Sigma-Aldrich), Potassium Iodide (Merck), Iodine (Merck), Ethylene Glycol (Alfa Aesar, 99%). Anatase P25 was obtained from Degussa. Fluorine doped tin oxide (FTO) coated glass (surface resistivity ≈8Ω/sq) was obtained from Aldrich.

1.2. Synthesis

Mesoporous Titanium Dioxide

The sol-gel synthesis of mesoporous TiO_2 is based on the procedure described elsewhere [1]. Briefly, 4.2g of titanium(IV) tetraethoxide (TEOT) were dissolved in 3.2g of concentrated hydrochloric acid at room temperature, under vigorous stirring. After approximately 5 minutes, a solution of 1g of P123 dissolved in 12g of ethanol was added. The solutions were aged for 10 minutes, at room temperature, under stirring.

To obtain the TiO_2 powder, this final solution was first dried by sintering the powder at 120ºC for 1h, heating rate= 60ºC/h. Once dried the samples were calcined at 400, 520 or 625ºC, for 4 hours, using a heating rate of 1ºC/min for samples produced at 400 and 520ºC and 2ºC/min for samples produced at 625ºC.

Synthetic and natural dyes

Synthetic dye solution was prepared adding 3',4',7-trihydroxyflavylium, synthesized in a previous work [2], to ethanol pH 1.0 (adjusted with HCl 1M) giving a final concentration of $5x10^{-4}$ M.

Natural dye solutions were obtained adding 5g of the residue, as sent by the companies, to 50mL of ethanol pH 2.0 (adjusted with HCl 1M), under stirring and heating of 40ºC, for 3 hours. After the extraction the solutions were filtered (GVS Laboratory Filtration, syringe filter, 0.25 mm, PE 0.50 µm).

Pre-treatment of the FTO glass

The treatment of the glass slides was performed using a titanium isopropoxide solution as suggested elsewhere [3]. Briefly, 0.71g of titanium isopropoxide and 0.07g of HCl were added to 8 mL of ethanol. After spin-coating of this solution the layer was dried at 150ºC for 30 minutes.

Electrolyte Solution

The iodide electrolyte solution was prepared by adding 0.5 M of potassium iodide mixed with 0.05 M of iodine in water-free ethylene glycol.

1.3. Characterization techniques

Dynamic Light Scattering (DLS)

DLS experiments were performed on a Horiba SZ-100, Horiba Scientific, cuvette cells and sample volume: 1-3 mL were used. The measurements were performed considering the viscosity of ethanol and using different temperature values: 25, 30, 35, 38, 43 and 45ºC. All the samples were previously filtered with a 0.45 µm pore filter (Life Sciences, GHP Acrodisc 13 mm, 0.45 µm GHP membrane). The mean particle size value was calculated assuming a Lognormal fit. DLS technique allows the determination of diffusion coefficients Diff, which can be afterwards used to calculate particle size.

X-Ray Diffraction (XRD)

XRD measurements were performed on a powder X-Ray Diffractometer RIGAKU, model MiniFlex II, 30kV/15mA, with copper X-Ray tubes, 5º - 80º (2Θ) and scanning speed: 1º/min.

Nitrogen Gas Porosimetry

N2 porosimetry measurements were performed on a Gas porosimeter, Micromeritics, model ASAP 2010.

Differential Scanning Calorimetry (DSC) and Thermogravimetric Analysis (TGA)

DSC and TGA analysis were performed on powders with a Simultaneous Thermal Analyser STA 449 F3 Jupiter. The scan temperature was between 25ºC and 700ºC and the scan rate used was 10ºC/min.

Transmission Electron Microscopy (TEM)

Transmission Electron Microscopy images were obtained with a Hitachi 8100 with TermoNoran light elements EDS.

Scanning Electron Microscopy (SEM)

The TiO_2 film surface morphology was analysed by field-emission gun scanning electron microscopy (FEG-SEM), JOEL 7001F with Oxford light elements EDS detector, at 15.0 kV.

UV-Vis Spectroscopy

The optical transmittance measurements were performed using a UV-Vis spectrophotometer Cary 300 Bio in the wavelength range from 200 to 800 nm. All the spectra were collected at room temperature.

Reflectance Spectroscopy

TiO_2 powders from the photodegradation experiments were analysed by reflectance spectroscopy on a UV-Vis spectrophotometer Shimadzu UV-2501 PC in the wavelength range from 250 to 800 nm.

1.4. Photodegradation experiments

The photodegradation experiments were based in the methodology developed elsewhere [4]. To follow dye adsorption we added 250 mg of the synthesized TiO_2 powder (calcined at 400ºC) to a solution of 10 mL of the grape dye extracted and 20 mL of ethanol (pH 2.0). We placed it under vigorous stirring, in the dark and followed the reaction for 3 hours. Small aliquots of the solution (≈2 mL) were taken at predetermined time intervals, centrifuged (Tehtnica Centric 150) and the supernatant was analysed by UV-Vis spectrophotometry. To perform the leaching-out test we added 150 mg of the coloured powder obtained to 20 mL of milli-pore water. The procedure was the same under stirring, in the dark and followed the reaction during 2 hours, collecting aliquots, centrifuging and analysing the supernatant by UV-Vis spectrophotometry. Finally, the irradiation step was performed adding 30 mg of the coloured powder to 6 mL of milli-pore water and irradiating the sample at 546 nm with a Xe/ Hg lamp (300W) under stirring, for 5 hours. The powder was then collected, dried and analysed. To produce the pellets for Reflectance analysis 2.7 mg of the powder sample was mixed with 145.2 mg of KBr. The powders were then mixed and ground together to produce a homogenous pellet.

1.5. Photochemical Devices

1.5.1. Deposition Technique

Spin-coating

The films were deposited using a SCS – Speciality Coating Systems G3P-8 spin-coater. The conditions used were as follows: Step: 1, Ramp: 1.0 seconds, Dwell: 30 seconds, Disp.: None. The treatment solution was deposited using RPM: 500 rpm, and the TiO_2 layer using RPM: 600 rpm.

1.5.2. Dye-Sensitized Solar Cells' Assembly and Characterization

The development of our DSSCs was based in the lab work procedure settled elsewhere [5]. The first step was to deposit the TiO_2 in the FTO glass slide. As explained before, a treatment of the glass using a solution of titanium isopropoxide was performed previous to the TiO_2 deposition. These samples were calcined at 400ºC, for 4h, heating ramp= 1ºC/ min. After this, the samples were sintered at 450ºC for 30 min to further eliminate any residues of organic matter that could still be present. These TiO_2 coated glass slides were left soaking in the dye solutions over-night. The carbon-coated counter electrode was prepared as suggested, covering the conductive side of the glass slide with a light carbon film, using a pencil. The cell was assembled using an iodide electrolyte solution as a relay agent. The cell was illuminated with an OSRAM Ultra-vitalux (300W) lamp.

- **Efficiency tests**

The efficiency tests were performed by LEPABE – Laboratory for Process Engineering, Environment, Biotechnology and Energy, Faculty of Engineering, University of Porto, in partnership with Dr Luisa Andrade and Dr Cláudia Costa.

2. Introduction

With the development of human society and the ever-growing need for better therapies for rare diseases, cleaner energy, reduce our environmental footprint and have safer, cleaner and more efficient industrial manufacturing processes, biotechnology provides tools to develop breakthrough products and technologies to tackle those problems and necessities. Biotechnology is, basically, technology based on biology, whether it is by using intact organisms (yeasts and bacteria), or natural substances from organisms, or even mimicking natural biomolecular processes. [6] Nature has already provided cells and living beings with all the essential tools to thrive and survive, it is now in our hands to be inspired by Nature and develop technologies and products that help improve our lives and the health of our planet.

One area of Biotechnology is Biomimetics. Biomimetics or Biomimicry concerns the understanding and adaptation or imitation of biological functions, structures and mechanisms of various objects found in Nature with the aim of designing and fabricating materials and devices of commercial interest and utility. There is a wide variety of objects in Nature to serve as inspiration, from bacteria to plants and animals. [7,8]

Plants are among the group of organisms, so-called photoautotrophs, which can perform photosynthesis. Photosynthesis is a process where solar energy harnessed from sunlight is used to produce chemical energy to drive the biochemical machinery of plant cells. This process is led by a complex set of molecular ensembles present in plant leaves, which comprises light-harvesting molecules, such as chlorophyll, arranged within the cells. Chlorophylls are not the only pigments present in Nature. [9] Another important group of pigments are anthocyanins, which belong to the flavonoids family and are responsible for the wide range of blue, purple and red colours seen in flowers, fruits and vegetables. Besides of their antioxidant power, the colours from anthocyanins are what attract pollinators and helps plants to reproduce, thus also playing a major role in plants survival. [9] From violet petals to the autumn leaves, from berries to grapes, anthocyanins present themselves as versatile compounds that can change their colour (by means of structural variations) depending on external *stimuli* such as pH, temperature and light. [10]

Due to the increasing use of energy, which is leading to many serious problems such as global warming and atmospheric pollution, the availability of the current main energy source, fossil fuel, is limited and will run out. Therefore, technology based on the photosynthetic process is being exploited to develop dye-sensitized solar cells to produce energy from a renewable energy source: sunlight. Sunlight is by far the largest available energy source. The energy from the sunlight that strikes the Earth, in one hour, is more than that consumed in the whole world for one full year [11,12]. Therefore one of the main objectives must be the production of technologies that mimic plants and perform light-harvesting, as well as the conversion of sunlight into energy. Direct conversion of sunlight into electricity can be achieved using a photovoltaic (PV) device, also called

solar cell. These devices can generate electricity directly from light without emissions, noise or loss of energy in any other form [11–13].

In this work we suggest not only the production of a Dye-Sensitized Solar Cell, to harvest and produce energy from sunlight, inspired in photosynthesis, as well as we intend to do so using natural occurring dyes, such as anthocyanins. We will obtain these anthocyanins by extraction from wine and olive oil productions' waste. Our aim is not only to provide a renewable and eco-friendly energy source by mimicking what happens in Nature, but also to give a new life to waste products and, from them, obtain and use natural resources (such as natural pigments) to attain it.

2.1. Dye-Sensitized Solar Cells

2.1.1. Operational Principle

Similarly to what happens in Nature during photosynthesis, Dye-Sensitized Solar Cells (DSSC), as described by Brian O'Regan and Michael Grätzel [14], are photovoltaic devices that use molecular dyes attached to titanium dioxide nanoparticles to produce energy from light harvesting. These devices use, for example, nanocrystalline inorganic oxides such as TiO_2, that are created using low-cost processes of fabrication without the expensive and energy-intensive high-temperature and high-vacuum processes needed for the traditional devices. These devices have a large flexibility in shape, colour and transparency, compatibility with flexible substrates and a large variety of presentations to facilitate market entry [14–16]. DSSCs differ from the conventional photovoltaic devices in that they separate the function of light absorption from charge carrier transport. A schematic representation of a DSSC is pictured in Figure 1. The mesoscopic semiconductor oxide film, TiO_2 is in contact with a redox electrolyte, iodide/triiodide (I^-/I_3^-) couple (relay agent). Attached to this film is a monolayer of the charge-transfer dye (D, here represented as the 3',4',7-trihydroxyflavylium molecule). Photoexcitation of the dye (Eq. 1) results in the injection of an electron into the conduction band of the semiconductor (Eq. 2a). The deactivation reaction (Eq. 2b) is a relaxation of the excited states, which occurs in competition with the electron injection into TiO_2. After the electron injection into the conduction band of TiO_2, the original state of the dye is restored by electron donation from the electrolyte (Eq. 3a). This regeneration of the sensitizer by the electrolyte (present at high concentrations) intercepts the recapture of the conduction band electron (e^-_{cb}) by the oxidized dye (Eq. 3b), avoiding energy-loss from this recombination, this way not limiting the photovoltage. The iodide is in turn regenerated by the reduction of triiodide at the counter-electrode (Eq. 4a), the circuit being completed via electron migration through the external load. Another recombination process that affects the current production of the cell is the capture of the conduction band electron of TiO_2 by the oxidized redox couple (Eq. 4b).

D + hv → D* (1)

$D^* + TiO_2 \rightarrow D^+ + e^-_{cb}$ (TiO_2) (2a)

$D^* \rightarrow D$ (2b)

$2\ D^+ + 3\ I^- \rightarrow 2\ D + I_3^-$ (3a)

$D^+ + e^-_{cb}\ (TiO_2) \rightarrow D + TiO_2$ (3b)

$I_3^- + 2\ e^-$ (catalyst) $\rightarrow 3\ I^-$ (4a)

$I_3^- + 2\ e^-_{cb}\ (TiO_2) \rightarrow 3\ I^- + TiO_2$ (4b)

The incident photon-to-current efficiency (IPCE) value corresponds to the photocurrent density produced in the external circuit under monochromatic illumination

$$IPCE = \mathrm{LHE}(\lambda) \times \Phi_{inj} \times \eta_{coll} \quad (5)$$

where LHE(λ) is the light-harvesting efficiency for photons of wavelength λ, Φ_{inj} is the quantum yield for electron injection from the excited sensitizer in the conduction band of the semiconductor and η_{coll} is the electron collection efficiency. The overall light-to-electrical energy conversion efficiency (η_{global}) of the dye-sensitized cell can be calculated by

$$\eta_{global} = \frac{V_{oc} \times J_{sc} \times FF}{I_s} \quad (6)$$

where V_{oc} is the open-circuit photovoltage, J_{sc} is the current measured at short circuit, FF is the fill factor of the cell and I_s is the intensity of the incident light. FF can vary from values between 0 and 1 and is defined by the ratio of the maximum power point (P_{max}) of the solar cell divided by the open-circuit voltage (V_{oc}) and the photocurrent density (J_{sc}). The P_{max} value is the point of maximum power output given by the J_{sc}-V_{oc} curves.

$$FF = \frac{P_{max}}{V_{oc} \times J_{sc}} \quad (7)$$

The photovoltage generated by the cell under illumination corresponds to the difference between the Fermi level of the electron in the semiconductor and the redox potential of the electrolyte. Overall, electric power is generated without permanent chemical transformation. [14–22]

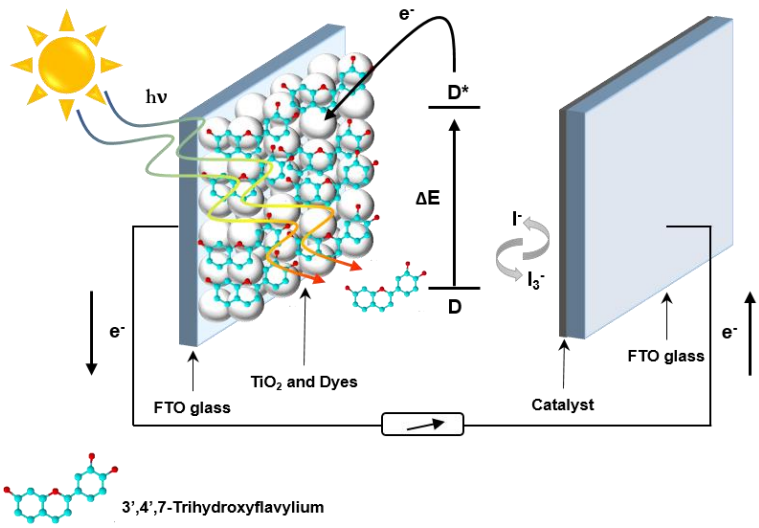

Figure 1. Schematic representation of the principle of operation of a Dye-Sensitized Solar Cell. The dye-sensitizer represented is the synthetic flavylium 3',4',7-trihydroxyflavylium.

2.1.2. Semiconductor oxide film

One of the most innovative aspects of DSSCs is the use of a mesoscopic semiconductor oxide film as the charge-carrier transporter. Mesoscopic materials have sizes normally larger than atoms but smaller than materials with micrometres. Mesoscopic materials, such as TiO_2, present great advantages. At the mesoscopic scale there is a significant increase of surface area. Mesoscopic TiO_2 presents a highly increased surface area when compared with its bulk analogue. This is one of the main reasons why mesoscopic materials attract scientific attention. [23,24] Another aspect that characterizes the normally used semiconductors is the wide band-gap. The band-gap in a solid is a range of energies (between the valence and conduction bands) where there are no orbitals and therefore, where no electrons can exist. [25] There are various wide band-gap oxides that can be used for this application, such as ZnO, SnO_2 and Nb_2O_5, but the most widely used has been TiO_2. Titanium dioxide has many advantages since it is cheap, abundant, nontoxic and biocompatible, being used in various applications, from treatment of environmental pollution, photoassisted degradation of chlorine compounds and phenol [26], paints and healthcare products. It is extensively studied for its electric, magnetic, catalytic and electrochemical properties. [16,18,27] TiO_2 occurs in three crystalline phases: rutile (tetragonal), anatase (tetragonal) and brookite (orthorhombic), all of which have Ti in an octahedral coordination with respect to O –, Ti^{4+} is present as $[TiO_6]$ octahedra. Brookite is the most difficult to synthesize due to its metastability. Both anatase and brookite can be transformed in rutile by phase transition at high temperatures (around 700ºC for anatase). [27–29] Although anatase and rutile are both fairly easy to synthesize in laboratory, anatase is more stable at low-temperatures and gives mesoscopic films that are transparent and colourless, with a wider optical absorption gap and a higher mobility of charge carriers than the rutile films. It also has a higher Fermi level than that of rutile by about ≈0.2 eV. In general, anatase is accepted as the more active of the two crystalline phases, both in photocatalysis and in photoelectrochemical studies, probably due to this difference in the Fermi

level. [17,27,30] Anatase has a wide band gap (≈3.2 eV) which makes it stable under illumination, and therefore it absorbs only in the UV part of the solar emission, making it insensitive to the visible spectrum, thus resulting in low conversion efficiencies (without sensitizer). These wide band-gap oxide films are insulating in the dark [15]. TiO_2 nanoparticles are deposited by, for example, screen-printing, doctor blading, spin-coating or inkjet onto a glass or flexible plastic support covered with a transparent conducting layer of fluorine-doped tin dioxide (FTO) or tin doped indium oxide (ITO). These nanoparticles are subjected to a short sintering or a calcining process to ensure that the particles are electronically interconnected (percolation) [16].

In terms of DSSC, the application of these type of semiconductors is of major importance. The mesoporous form of the semiconductors is much different from their compact analogues, and is what grants these DSSCs their highly efficient charge transport through the TiO_2 layer. Mesoporous films have a low inherent conductivity, the small size of the individual nanoparticles does not support a built-in electric field and the electrolyte penetrates the porous film all the way to the back-contact producing a junction of huge contact area. [16–18,22] The absorption of light by a dye-sensitized mesoporous semiconductor is more efficient than that by a monolayer of dye, resulting in a higher photovoltaic efficiency. When light penetrates the photosensitized semiconductor it crosses several adsorbed dye monolayers. Thus, the semiconductor structure simulates the thylakoid vesicles in green leaves, which are stacked in order to enhance light harvesting by chlorophyll. Since the nanocrystalline film function is to serve as an electron conductor, it is important that this transport occurs rapidly through the TiO_2 layer. This is one of the reasons these cells use an inorganic oxide instead of phospholipid membranes as in natural photosynthesis. The other is that these photovoltaic devices are supposed to remain serviceable for 20 years without significant loss of performance, and so inorganic oxides revealed to be a better option than phospholipid membranes. [16–18,22]

2.1.3. Dye Sensitization

Dye sensitization plays a crucial role in DSSCs since light absorption depends on it. The ideal sensitizer must fulfil certain requirements. The dye must absorb solar radiation strongly with absorption bands in the visible and near-IR region, preferably covering a wide range of wavelengths. It also should bind strongly to the semiconductor, thus it should carry attachment groups such as carboxylate, phosphonate, or hydroxyl to ensure efficient injection of the electron into the oxide conducting band and to prevent gradual leaching by the electrolyte. Electron injection into the TiO_2 must be very fast in comparison with the decay from the excited state to the ground state of the dye. The energy level of the excited state (LUMO) should be well matched with the lower bound of the semiconductor band of the oxide film to minimize energetic losses during the electron transfer. The HOMO of the dye should be sufficiently low in energy for efficient regeneration of the oxidized dye by the redox couple. Finally, and in contrast with chlorophyll which is continuously being synthesized in the leaf, the sensitizer in the DSSC must be stable

enough to sustain at least 10^8 redox turnovers under illumination, which corresponds to 20 years of exposure to natural light without significant loss of performance. [2,16–18]

The most widely used dyes in DSSCs have been based in Ru complexes, since they had proven to be the most efficient sensitizers [2,16–18,22]. Since these dyes are based on expensive rare metals and require complex multistep synthesis involving toxic and environmentally harmful chemicals which are not sustainable for mass-scale application, various alternatives were studied. In the last couple of years a novel approach has been studied where a Pb based dye (however, still a toxic element), perovskite, has been studied and high efficiencies have been reported [31–33]. Besides of a wide variety of organic dyes [34], natural dyes have shown promising properties as efficient photosensitizers [2,35–40]. Natural dyes are an attractive option since they are easily available, non-toxic, low-cost, environmentally safe and totally biodegradable. Among the many available natural pigments, the three main families used to TiO_2 sensitization have been chlorophylls, betalains and anthocyanins [36,40].

Anthocyanins belong to the flavonoid family, and are the pigments responsible for the colours seen in a broad variety of flowers, fruits, vegetables and roots. From pink to red, violet and blue, anthocyanins present themselves as versatile compounds that can change their colour (by means of structural variations) depending on external *stimuli* such as pH, temperature and light. Effectively, what distinguishes anthocyanins from other flavonoids is not only the fact that they are coloured (while most flavones and flavonols are colourless), but also that they can change colour through a series of chemical reactions such as proton transfer, *cis-trans* isomerization and tautomerization. The core structure in anthocyanins is the 2-phenyl-1-benzopyrylium carbon skeleton (flavylium cation) which bears hydroxyl, methoxyl and/or glycosyl groups. Natural anthocyanins possess one or more sugar units, being the most frequently encountered the β-D-Glucose, β-D-Galactose and α-L-Rhamnose. [35,41,42] Figure 2A pictures the structure of a natural anthocyanin (chrysontemin) and of a synthetic flavylium cation.

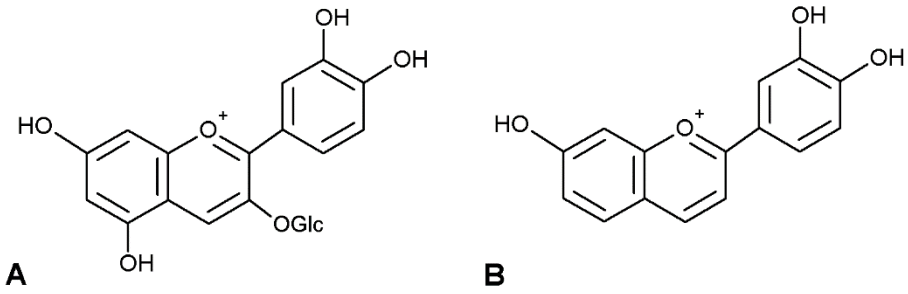

Figure 2. A- Molecular structure of cyanidin-3-glucoside (chrysontemin), a natural anthocyanin.
B- Molecular structure of 3',4',7-trihydroxyflavylium cation.

Natural occurring dyes develop through Nature's evolution process, optimizing and rearranging according to its needs. However, it is sometimes useful to control and rearrange the molecule we are working with to optimize the outcome of the experiment. For DSSCs purposes, for example,

it is possible to follow a bio-inspired strategy and with the adequate structural modifications prepare quasi-natural biomimetic compounds. This is the case of flavylium compounds. With simple, non-toxic and environmentally safe synthetic procedures it is possible to design and prepare compounds with similar properties of natural occurring anthocyanins. Synthetic flavylium ions are constituted by the same carbon skeleton as anthocyanins and the optimization process is made through substitution of adequate groups in the core structure of the dye tailoring desired energy levels and absorption properties. [2] Figure 2B represents one of these synthetic flavylium compounds, 3',4',7-trihydroxyflavylium, designed and optimized to use in DSSC studies [2].

2.1.4. Development of a DSSC

In this work we propose the development of a dye-sensitized solar cell. We will study and optimize a sol-gel method of TiO_2 synthesis and produce films by spin-coating deposition on top of an FTO conducting glass.

Spin-coating is one of the most widely used deposition techniques for the development of solar cells. This technique allows highly reproducible and homogeneous films. The principle of operation is based on centrifugal force: an excess amount of the desired solution is placed on top of the substrate, which then is accelerated to a predefined rotational speed as shown in Figure 3. The angular velocity of the substrate results in the ejection of most of the applied solution, forming a thin and uniform film. Simultaneously, the solvent in the solution evaporates. The final film thickness depends on the angular velocity of spinning (the higher the velocity, the thinner the film), as well as on the viscosity and concentration of the solution and solvent. Spin-coating technique is highly reproducible when working with small substrates, meaning it is a good technique to apply on a laboratory scale. However, for commercialization of DSSCs, where mass and large-scale production is required, this technique becomes uncompetitive. Due to the difficulty to deposit large area films and solution waste among others, this technique shows limited conditions for being applied at an industrial level. [43,44]

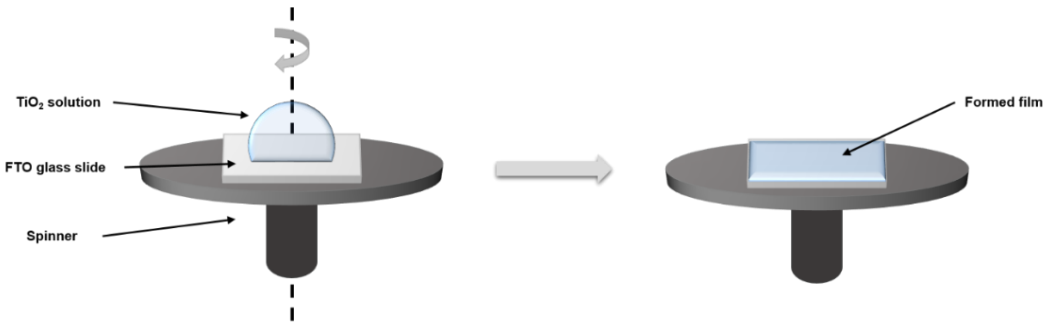

Figure 3. Schematic representation of the spin-coating technique. An excess amount of volume of the sol-gel solution is placed on top of the glass (substrate). The spinner starts rotating at a predefined velocity and the solution spreads throughout the surface of the glass forming a uniform film.

We will work with three different dye sensitizers: 3',4',7-trihydroxyflavylium, a synthetic analogue of anthocyanins which has already given proof of being a good dye-sensitizer for DSSC application [2], and pigments extracted from two natural sources - biological waste from wine and olive oil industries.

As explained before, anthocyanins are the molecules responsible for the great majority of the colours seen in Nature. Grapes [36,40,45,46] and olives [47–51] are among the many fruits, flowers and vegetables that owe their strong colour to anthocyanins. Between the various pigments found in grapes and olives, cyanidin-3-glucoside, malvidin-3-*O*-rutinoside and malvidin-3-*O*-coumaroylglucoside are known to be responsible for the purple colour of grapes, and cyanidin-3-*O*-glucoside and cyanidin-3-*O*-rutinoside are pointed as being responsible for the black colour of olives. There are inclusively reported works where grape's pigments were used as sensitizers in DSSCs [36,40,45]. Since Portugal is a country with wine and olive oil production, and being aware of the continuous and ever-growing need to reutilize and recycle compounds and materials, we decided to build a DSSC based on biological waste residues instead of using fresh fruit. Two different companies provided us with the final biological waste of their production, one from red wine production and the other from olive oil production, for us to perform the pigments' extraction and use as sensitizers in the DSSCs.

Figure 4 shows a schematic representation of our proposed dye-sensitized solar cell. As explained, the substrate for the dye-sensitized semiconductor is a glass with a conducting layer (FTO). The TiO_2 layer is deposited, followed by the adsorption of the dye-sensitizer. An electrolyte, with the I^-/I_3^- redox couple, is placed in contact with the semiconductor, so it can penetrate through the film pores and re-establish the sensitizer's electrons after photoexcitation. Finally another conducting glass with a catalyst (e.g. carbon) is placed to seal the cell, this counter-electrode also has the function of regenerating the redox couple.

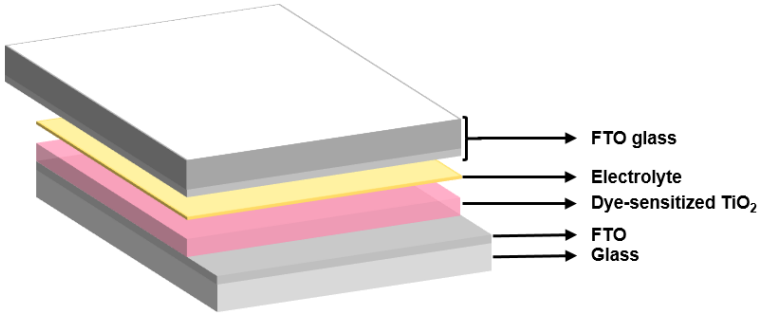

Figure 4. Schematic representation of the DSSC based on dye-sensitized TiO_2.

2.2. Photodegradation using TiO_2 as a Catalyst

During photosynthesis plants capture energy from sunlight to produce oxygen and carbohydrates by oxidizing water and reducing carbon dioxide (Eq. 8). In photodegradation processes, in this case photocatalysis, the opposite reaction is promoted. By using a semiconductor as a catalyst, such as TiO_2, and a source of photons (UV lamp or sunlight), a series of oxidation processes are initiated that can remediate contaminated samples until mineralisation, meaning organic compounds may be degraded to CO_2, H_2O and other inorganic species. This type of remediation process (photocatalysis) has been the target of many attention for the last decades, focusing on the possibility of using this process to remediate, for example, contaminated waters.[52]

$$6\ CO_2 + 6\ H_2O \xrightarrow{h\nu} \text{Glucose} + 6\ O_2 \qquad (8)$$

Titanium dioxide has been extensively studied to perform the catalyst role. [53] Once again, its high photosensitivity, non-toxicity, easy availability, low-cost, strong oxidizing power and long-term stability have been detrimental in this choice. However, its photocatalytic activity remains insufficient for practical application. Because of the recombination of electron-hole pairs after the irradiation of TiO_2 with energy equal to/or higher than its band gap, the photocatalytic efficiency is reduced. [54] Furthermore, and as previously explained, due to its wide band-gap, TiO_2 can only absorb light in the UV region. Since only less than 5% of the solar light that reaches the Earth is in the UV region, this process is limited right from the beginning, thus not allowing an effective use of sunlight to drive the reaction when pure TiO_2 is used as a catalyst. To be viable the application of this remediation process for the degradation of organic pollutants, for example, it is more desirable to use visible light as the energy source. [55]

Several strategies have been developed to overcome these drawbacks. To minimize or avoid the effect of recombination, several studies have been developed where, in association with TiO_2, metals or other semiconductors were used to form heterostructures [54,56–59]. The strategy to extend the photo-response of TiO_2 to the visible region is based on the principle of DSSCs. By means of dye-sensitization of TiO_2 (adsorbing a dye into the TiO_2) visible light harvesting is made possible. In this strategy, and as happens in DSSCs, TiO_2 has the 'charge-carrier' function. The dye molecules act as *antennae* to absorb the light energy into the degradation system. The principle of operation is the same: photoexcitation of the dye (Eq. 1) results in the injection of an electron into the conduction band of the semiconductor (Eq. 2a). In presence of O_2 the existing pollutants, or the adsorbed dye itself (in case this is the target), can be oxidized to CO_2, H_2O and other products. Organic compounds, as well as dye pollutants from the textile industry, are sources of environmental contamination and are potential targets for this type of photocatalysis. [55,60]

In Chapter 2.3. Photodegradation of Biological Waste Compounds using TiO_2 as a Catalyst we develop this concept of enhanced photo-response of TiO_2. By adsorbing the pigment extracted from the wine waste sample into the TiO_2, in presence of O_2 and photo-irradiation in the visible region, we aim to degrade the dye adsorbed and prove the concept presented above.

3. Results and Discussion

3.1. Nanoparticle synthesis

Titanium dioxide was extensively studied since it is a wide band-gap semiconductor, non-toxic, photo-stable, cheap and very efficient under UV light. These characteristics make this compound the choice when it comes to applications such as photovoltaic cells, electrochromic devices, sensors, membranes, as a catalyst in various reactions (principally as a catalyst to photodegradation studies), among many others. In this work we synthesize mesoporous TiO_2 powders to use in various applications. Several methods for titanium dioxide synthesis were tested during this work. The first approach was to synthesize TiO_2 mesoporous single-crystals (MSC's) using Silica templates [3]. This method intended the growth of semiconductor MSC's of TiO_2 (anatase) based on seeded nucleation and growth inside a mesoporous template (Silica) by immersion of this template in a dilute reaction solution. This nucleation and growth process used two different TiO_2 precursors: $TiCl_4$ and TiF_4. We struggled to reproduce the results reported since this synthesis method is very complex and comprised a great amount of different steps, reagents and time. A second very different approach was studied, with the production of Ti-MCM-41 samples [61]. This method used MCM-41, a well-studied ordered mesoporous structure, for the introduction of Titanium and Silica. The precursors are, respectively, TEOT and TEOS. We were able to reproduce the synthesis and obtain a sample with approximately 50% Si/Ti ratio. Since the final purpose of this work was to synthesise pure TiO_2 (anatase) this method was discarded. Nonetheless, this method functioned as inspiration to continue working with templates, such as MCM-41, to serve as guides for titanium deposition. Focusing on another well-studied templating agent, Pluronic P123, the method described by Peter C. A. Alberius *et al.* [1] was studied. Synthesis method and further studies, optimizations and characterizations are presented below.

3.1.1. Nanoparticle Growth

The sol-gel synthesis used in this work is based on the procedure developed elsewhere [1]. This synthesis method, besides of using simple methods and techniques, uses a small number of reagents and the overall process comprises a short amount of time. These facts make it a low-cost method of synthesis. This sol-gel synthesis uses a surfactant, Pluronic P123, as the template for the deposition of TiO_2 obtained from the TEOT solution used. This solution was aged at room temperature (according to the defined protocol) for 10 minutes, under stirring. The first step was to study the influence of temperature on nanoparticle formation and growth (between room temperature and 45ºC). We used Dynamic Light Scattering (DLS) to follow the kinetics of this reaction.

Dynamic Light Scattering is a technique where a monochromatic beam of laser light impinges on a sample and is scattered by the particles in solution into a detector. The result presented by this

technique in an autocorrelation function (ACF). An ACF is the autocorrelation of the fluctuations in the intensity of light dispersed by the particles in the solution. From these results a diffusion coefficient (Diff) is measured. From this diffusion coefficient the size of the particles dispersing light can be calculated. The principle of DLS is based in the fact that small particles in suspension undergo random thermal motion known as Brownian motion. This random motion is modelled by the Stokes-Einstein equation (Eq. 9). Stokes-Einstein equation can then be applied to calculate the average particle diameter D_h,

$$D_h=\frac{k_{B\times}T}{3\pi\times\eta\times Diff} \qquad (9)$$

where k_B is the Boltzmann constant, T is the temperature (K), η is the solvent viscosity and Diff is the diffusion coefficient obtained by DLS. [62]

Figure 5 shows the autocorrelation functions (ACF's), obtained from the DLS measurements, for three of the temperatures studied (25, 35 and 43ºC) from the beginning of the sol-gel reaction until a final stable state is reached. An increase of intensity of the autocorrelation function is observed from the beginning of the sol-gel reaction to the final state. Also the results give evidence of the presence of a relaxation with two components when the ACF is plotted in a logarithmic scale vs. correlation time now in a linear scale (Figure 6). In the beginning of the sol-gel reaction, a bi-exponential relaxation is observed clearly. These results corroborate the idea that shorter relaxations can be assigned to micelles and longer relaxations are due to TiO_2 nanoparticles' growth, resultant from TiO_2 deposition on the micelles' surface. As the system evolves, the faster relaxation times disappear as a result of nanoparticle growth, and only the relaxation of the TiO_2 nanoparticles remains.

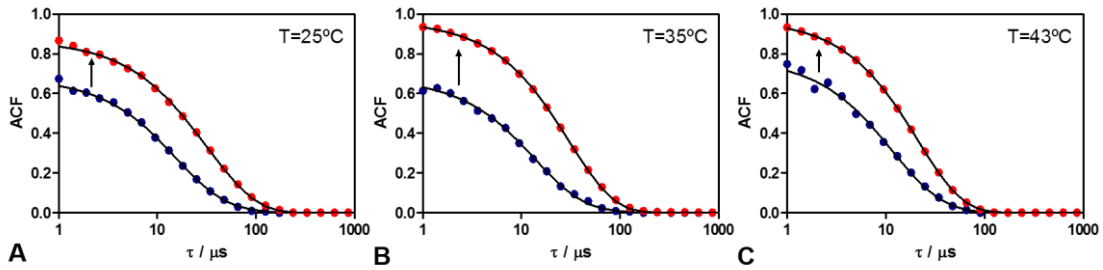

Figure 5. Autocorrelation function (ACF) curves obtained from DLS measurements performed at 25ºC (A), 35ºC (B) and 43º (C). Inserts: Beginning of the sol-gel reaction (●), final stable state (●).

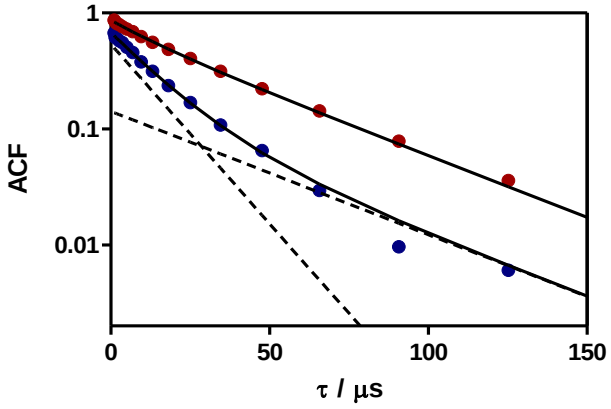

Figure 6. ACF curves obtained from DLS measurements performed at 25ºC, applying the logarithmic scale in the ACF axis. Inserts: Beginning of the sol-gel reaction (●), final stable state (●).

Figure 7 shows how the nanoparticles grow at two different temperatures (25 and 43ºC). At 43ºC nanoparticles reach their final size much faster than at room temperature, where it takes the nanoparticles 2h to reach that same final size. The particles volume (V_h) growth with time is approximately single-exponential, therefore it follows a pseudo-first order kinetics, which means that the velocity of the reaction depends directly on $Ti(OH)_4$ concentration. Thus implying that increasing the concentration of $Ti(OH)_4$ will increase the rate of the reaction. Equation 10 is the exponential equation used to adjust the results obtained, where V_{calc} is the exponential that fitted the results, V_{final} is the final volume reached by the nanoparticles, V_0 is the initial volume of the nanoparticles, t is the time took following the reaction (x axis of Figure 7) and $t_{reaction}$ is the time it took for the reaction to reach a final stable state. Parameters V_{final}, (V_{final}-V_0) and $t_{reaction}$ were adjusted using the Solver tool.

$$V_{calc} = V_{final} - (V_{final} - V_0) \times exp^{-\frac{t}{t_{reaction}}} \qquad (10)$$

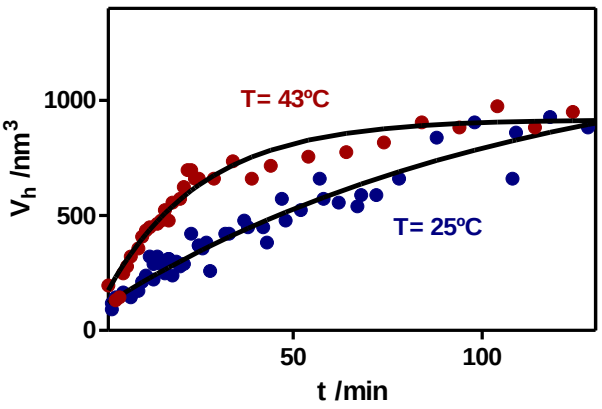

Figure 7. Titanium dioxide nanoparticles' growth, represented by their volume in function of time, at two of the studied temperatures 25ºC (●) and 43ºC (●).

Table 1 presents the results obtained for the velocity of the reaction (k_{obs}) in terms of the temperature of reaction (T), and the respective final hydrodynamic diameter (D_h) of the nanoparticles. From the values presented the first conclusion we can draw is that temperature does not affect the final size of the nanoparticles. This is based on the fact that the final sizes achieved by the nanoparticles were all around the same value (mean value around 13.4 nm), and changing the temperature only affected the time necessary to reach that final size. Another evidence is that temperature affects the velocity of the reaction (k_{obs}), but only for temperatures higher than 35ºC, below that a 10ºC increase in temperature (from 25ºC to 35ºC) resulted in an increase of only 0.0035 min^{-1}, whereas from 43ºC to 45ºC, a difference of only 2ºC, resulted in an increase of 0.0233 min^{-1}.

Table 1. Values calculated from the results of the DLS measurements.

T /ºC	1000/T /K^{-1}	k_{obs} /min^{-1}	D_h^{final} /nm
25	3.35	0.0091	13.4
30	3.30	0.0091	14.3
35	3.25	0.0126	15.1
38	3.21	0.0261	11.9
43	3.17	0.0398	12.1
45	3.14	0.0631	13.6

Dynamic light scattering enabled the comprehension of titanium dioxide's formation and nanoparticle growth, and allowed the formulation of a mechanism for this reaction. Figure 8 shows a schematic representation of the steps involved in this process. Pluronic P123 micelles work as precursors for TiO_2 deposition through a condensation process. Once the sol-gel solution is obtained, with the grown nanoparticles in suspension two things can be done: dry the sol-gel solution to give rise to a powder (this is the step followed in this work), or leave the solution to further react and give rise to a gel, through a gelation process.

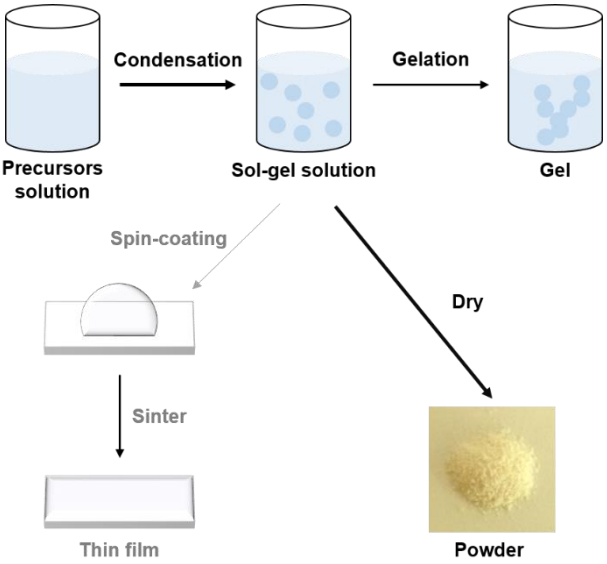

Figure 8. Schematic representation of sol-gel synthesis and the possible products.

According to the results obtained a model for the formation and growth of TiO_2 nanoparticles can be suggested. The reaction is performed in an acidic medium to slow the velocity of the gelation process thus preventing polymerization of the TEOT. We believe that the first reaction that occurs is the loss of the four ethoxide groups and consequent formation of titanium hydroxide (Eq. 11). This first reaction is thought to be very fast, probably occurring in less than 1 minute, thus not being itself measured in the DLS experiment. The second occurs through a condensation process (Figure 8) where titanium hydroxide molecules start to condense and give rise to TiO_2 (Eq. 12). This condensation process is believed to occur in the micelles' surface. $Ti(OH)_4$ molecules diffuse through the solution and partition to the pluronic micelles and there condense and give rise to the TiO_2 structure shown in equation 13. This reaction is thought to be favoured in the micelle's surface, and not in the solution. All these hypothesis are supported by the DLS results obtained. The exponential growth (Figure 7) and the fact that the final size of the nanoparticles (Table 1) is practically the same whatever the temperature of the reaction, confirm this model. If nanoparticle growth occurred by, for example, successive fusion of smaller nanoparticles, the kinetics would be of "n" order, and would not be described by an exponential. The k_{obs} values (Table 1) also support this model. With the increase in temperature, there is a decrease of the solvent's viscosity, this facilitates the diffusion of the molecules to the micelle's surface, consequently significantly increasing the rate of the growth reaction. For temperatures lower than 30ºC k_{obs} values are fairly constant. This can be explained by the fact that, at low temperatures such as 25ºC, since the diffusion of the molecules to the pluronic micelles is lower due to increased medium's viscosity, gelation processes may begin to occur in a small amount. Therefore, the observed constant remains practically the same, but with two different contributions: condensation processes (the great majority) and a small amount of gelation processes. This gelation processes, however, are not significant enough to affect the nanoparticles final size, since there is no great variation observed (Table 1).

$$Ti - (OCH_2CH_3)_4 + 4\ H_2O \rightarrow Ti(OH)_4 + 4\ Ethanol \quad (11)$$

$$2\ Ti(OH)_4 \rightarrow (TiO_2)_2 + H_2O \quad (12)$$

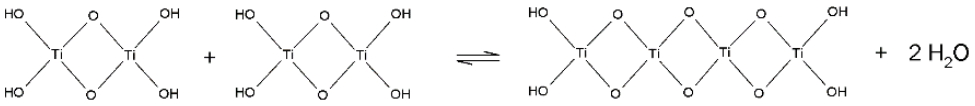

(13)

Since the final size of the nanoparticles is not affected by the temperature of reaction, and given the results obtained, we decided to perform the nanoparticles' growth reaction at 25ºC, since it is easier and cheaper in a practical point of view to work at room temperature.

3.1.2. TiO_2 Nanoparticles Characterization

After understanding the behaviour of the nanoparticle growth and the optimization of the sol-gel process in general, we decided to study the influence of the calcination temperature on the final powder characteristics. Three calcination temperatures were chosen 400, 520 and 625ºC to understand and explore the boundaries between amorphous to anatase and anatase to rutile crystalline phase transitions. Throughout the studies commercial anatase (Degussa P25) was used as a reference. Figure 9 shows the general aspect of the powders obtained and characterized.

Figure 9. A- TiO_2 nanoparticles before calcination, and after a short sintering process (120ºC, 1h and ramp: 60ºC/ h). **B-** Synthesized powder from calcination at 400ºC. **C-** Synthesized powder from calcination at 520ºC. **D-** Synthesized powder from calcination at 625ºC. **E-** Commercial anatase (Degussa P25).

X-Ray Diffraction (XRD)

An XRD analysis was performed (Figure 10) to assess about the crystallinity of the powders synthesized, using as a reference the XRD spectrum of the commercial anatase powder (Figure 10A). This commercial powder (Degussa P25) is a mixture of anatase and rutile phase of titanium dioxide in a 3:1 ratio [63]. All XRD spectra show well-defined diffraction peaks, although there is an increase in definition and the appearance of new peaks with the increasing in calcination temperature. The spectrum of the powder calcined at 625°C (Figure 10B) is more similar to that of the commercial powder, than those from 520°C (Figure 10C) and 400°C (Figure 10D). This is particularly evident at $2\theta \approx 27^{o}$ (where θ is the Bragg angle) where in samples A and B a well-defined peak is observed, but in samples C and D it is absent. This means that all the samples display the same crystallinity, the tetragonal anatase phase of titanium dioxide, but probably at 625°C the change to the rutile crystalline phase begins to be promoted. Samples C and D show all the peaks associated with the anatase phase (JCPDS No. 21-1272).

Another important aspect is the narrowing of the peaks with the increase in calcination temperature. The peak's width is related to the nanoparticle size by the Scherrer's equation,

$$D_{hkl} = \frac{K \times \lambda}{B_{hkl} \times \cos\theta} \qquad (14)$$

where D_{hkl} is the crystallite size (hkl are the Miller indices of the planes being analysed), K is a numerical factor frequently referred to as the crystallite-shape factor, λ is the wavelength of the

X-ray beam, B_{hkl} is the full width at half-maximum of the X-ray diffraction peak and θ is the Bragg angle [64]. Since the diffraction peaks are broader in sample D comparatively to the other samples, one can assume that the nanoparticles are smaller than, for example in sample B, where there is a noticeable straightening of the diffraction peaks. Thus, XRD analysis lead us to the conclusion that increasing the calcining temperature not only results in an increase of the nanoparticles' size, but also, for temperatures as high as 625ºC, anatase to rutile crystalline phase transition begins to be promoted.

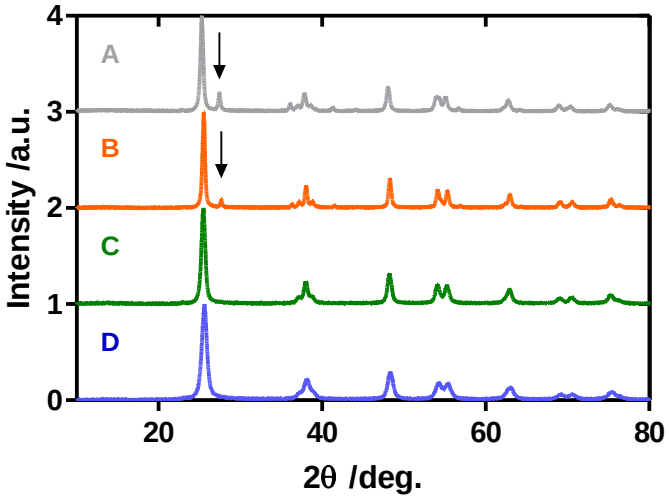

Figure 10. XRD spectra of the commercial anatase (**A**), synthesized powder calcined at 625ºC (**B**), synthesized powder calcined at 520ºC (**C**) and synthesized powder calcined at 400ºC (**D**). Insert: Peak at 2θ≈27 degrees.

Nitrogen Gas Porosimetry

To learn about the powders' characteristics in terms of surface area and pore size, N_2 Porosimetry analysis were performed. Table 2 summarizes the results obtained. The first major conclusion is that the powder synthesized and calcined at 400ºC shows significantly greater surface area and pore volume than the widely used commercial anatase (Degussa P25). The BET surface area of the powder synthesized is at least twice as great as that of the commercial powder, and the pore size is at least four times greater than that of the commercial powder. These are major results since this was one of the main objectives of this work, to produce a mesoscopic semiconductor TiO_2 powder competitive to what is usually used for most of DSSC studies. Another result that is evident is the relation between calcination temperature and the resulting surface area and pore volume. Since the calcination process promotes solvent and surfactant disappearance and increased crosslinking of the inorganic framework, it is normal to observe that the higher the calcination temperature, smaller the pore volume and consequently, lesser surface area. We can further relate these results with those obtained from XRD analysis. Since the higher the calcining temperature, the bigger the nanoparticles' size, it makes sense that the volume of the pores between nanoparticles decreases accordingly. Thus resulting in a decrease of the overall surface

area. This can also be evidence that the TiO_2 synthesized is not thermally stable, since once increased the calcination temperature, the pores are blocked and the surface area decreases rapidly [65]. When increasing the calcination temperature from 400 to 520ºC (an increase of 120ºC) there is a 24% decrease in surface area. With the second increase in temperature of only 105ºC, from 520 to 625ºC, a decrease of approximately 54% is seen, suggesting that the higher the temperature, the less stable the structure is. This decrease in the structure's stability leads to a collapse and consequently, to a decrease in surface area. An important conclusion we can draw from these results is that all the pore sizes observed are between 2-50 nm so, according to the IUPAC definition, this indicates the presence of mesoporous materials.

Table 2. Results obtained from the N_2 Porosimetry measurements.

Sample	BET Surface Area /$m^2.g^{-1}$	Pore Volume /$m^3.g^{-1}$	Pore Size /nm
TiO_2 400°C	106.4	0.385	14.5
TiO_2 520°C	80.7	0.281	13.9
TiO_2 625°C	37.4	0.170	18.2
Commercial TiO_2	47.3	0.088	7.5

This study allowed the confirmation of the results obtained in XRD analysis concerning the particles' size, and to determine that the powder that has the greater surface area and pore volume, hence the one that theoretically has the greater capacity to adsorb compounds (like dyes), is the powder calcined at 400ºC.

Thermal and Calorimetric Analysis

To evaluate the temperature at which anatase begins to crystallize, Differential Scanning Calorimetry (DSC) and Thermogravimetry Analysis (TGA) of the as-synthesized sol-gel TiO_2 nanoparticles were performed. Figure 11 shows the results obtained. Looking at the TGA curve there is a small decrease of about 3% of weight, right at the beginning, which probably represents the evaporation of residual water. Starting at about 200°C there is a clear decrease relative to a great amount of weight loss, around 34.7%, related to the removal of the block copolymer species from the TiO_2 structure. The weight decrease of about 6.2% between approximately 310ºC-700ºC can be attributed to the loss of residual surfactant still present in the TiO_2. The exothermic peak at 297ºC present in the DSC curve without any significant weight loss verified in the TGA curve, can most likely be attributed to the amorphous to anatase phase transition of TiO_2. The endothermic peak detected at approximately 440°C is probably related to the previously referred oxidation of block copolymer still present in the sample. Although in this measurement we reached temperatures as high as 700ºC we did not see the anatase to rutile phase transition expected based on the XRD results (where at 625ºC we started to have rutile). This shift to higher temperatures of the phase transition in the DSC results can most likely be attributed to the rapid

heating rate used, 10°C/min, opposed to the 2°C/min rate used in the calcination process, where the sample is further maintained at 625ºC for 4h.

Another DSC-TGA measurement was performed but this time on the anatase powder synthesized and calcined at 400ºC to see the phase transition from the anatase phase to rutile (Figure 12). There is an overall mass loss of about 3.8% probably associated with water evaporation from the powder, accompanied with an endothermic peak at about 51ºC. Since the powder was calcined at 400ºC this water must be from moisture contamination and not water entrapped inside the structure of the material or from its composition. There is no evidence of any phase transition, since no other peak is observed in the DSC curve. Again this can be attributed to the rapid heating rate applied in the DSC study (10ºC/min), in contrast with the 2ºC/min heating rate used to perform the calcination at 625ºC, where the sample is maintained at this final temperature for 4h. So, this DSC study could not be used to support the XRD results for the sample calcined at 625ºC, but we still believe that, because of the conditions used in the calcination process, we are promoting a change of phase from anatase to rutile.

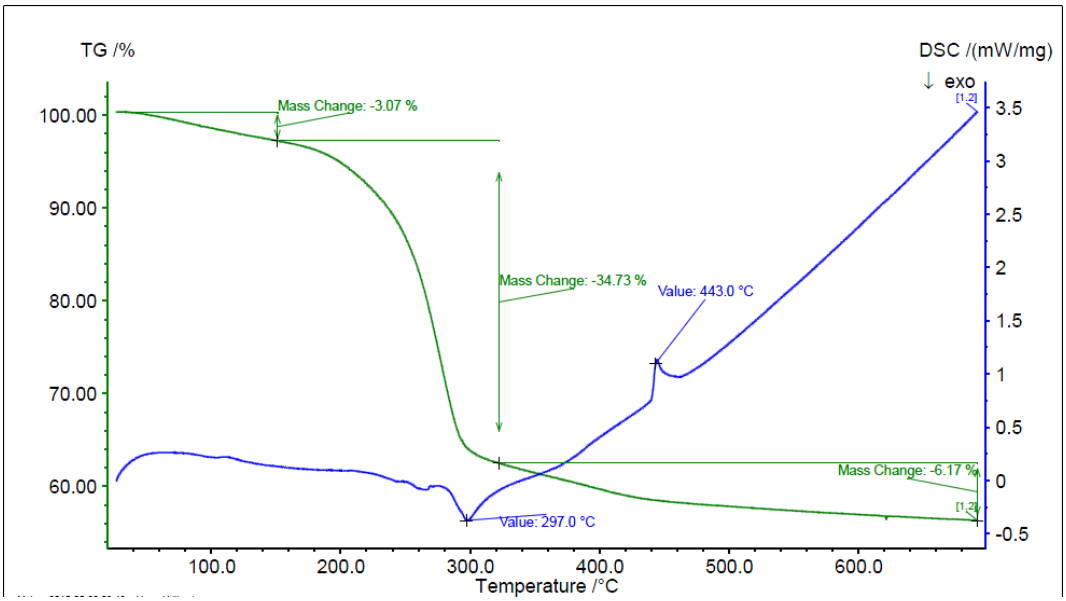

Figure 11. DSC (blue line) and TGA (green line) analysis of the TiO_2 sol-gel before the calcination step. Scan rate equal to 10ºC/min.

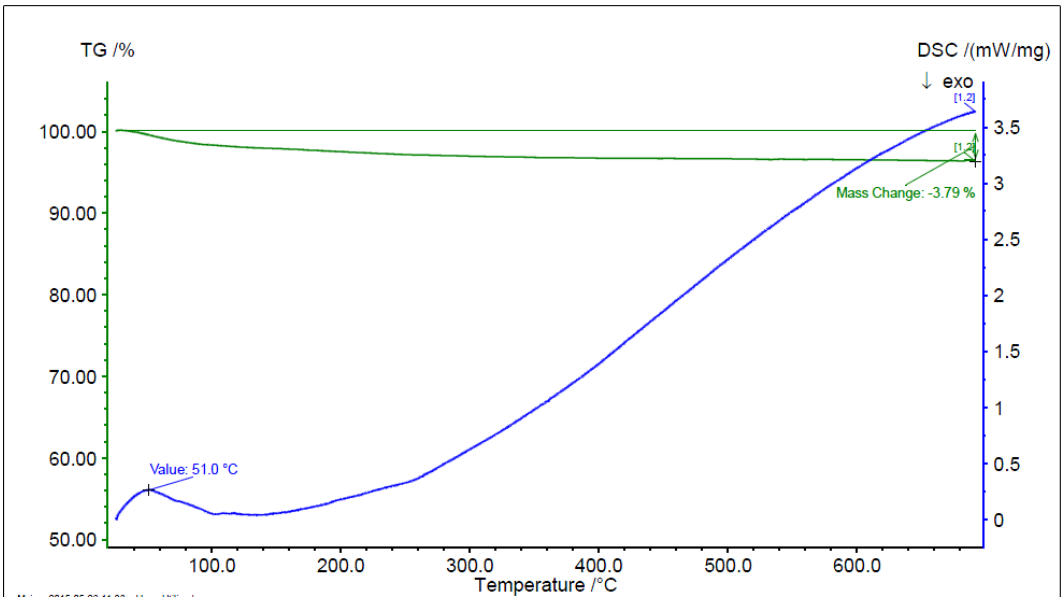

Figure 12. DSC (blue line) and TGA (green line) analysis of the synthesized powder calcined at 400ºC. Scan rate equal to 10ºC/min.

Transmission Electron Microscopy (TEM)

Figure 13 shows the images obtained from the TEM analysis. For each of the samples it is shown a first image with the overall aspect of the powder and a second one where it is possible to see the crystalline net of titanium dioxide. These later images support the results obtained by the XRD analysis, in proving that the nanoparticles synthesized correspond to a crystalline phase of TiO_2, and not the amorphous phase. This is a very important result. All the desired characteristics, above mentioned, for these TiO_2 powders are relative to the anatase crystalline phase of TiO_2. So guaranteeing the synthesis of a powder that presented a crystalline phase of TiO_2 (anatase) was of major importance. Another important aspect to retain is the “grey matter” surrounding the nanoparticles. It is possible to see that this background becomes less evident (less dark) with the increase of the calcination temperature. This grey matter is possibly organic matter (most likely surfactant) that was not removed from the powder, which makes sense since the DSC results showed that after that high peak of surfactant loss, there is a gradual, less abrupt, loss of organic material accompanying the temperature increase. TEM results also allow the observation that the sizes of the nanoparticles are polydispersed in all the samples, varying from nanoparticles with a size of about 50 nm to ones with probably less than 5 nm. In spite of this evident polydispersity there is a clear difference in the nanoparticles’ sizes. All the samples are shown in the same amplification to facilitate comparison. Looking at the images on the left (for samples A, B and C) there is a clear increase in the overall size of the nanoparticles with the increase in calcining temperature. This corroborates the results obtained from the XRD analysis. Finally, for all the samples, a general disorganization of the nanoparticles is seen, not showing any specific order or structured distribution.

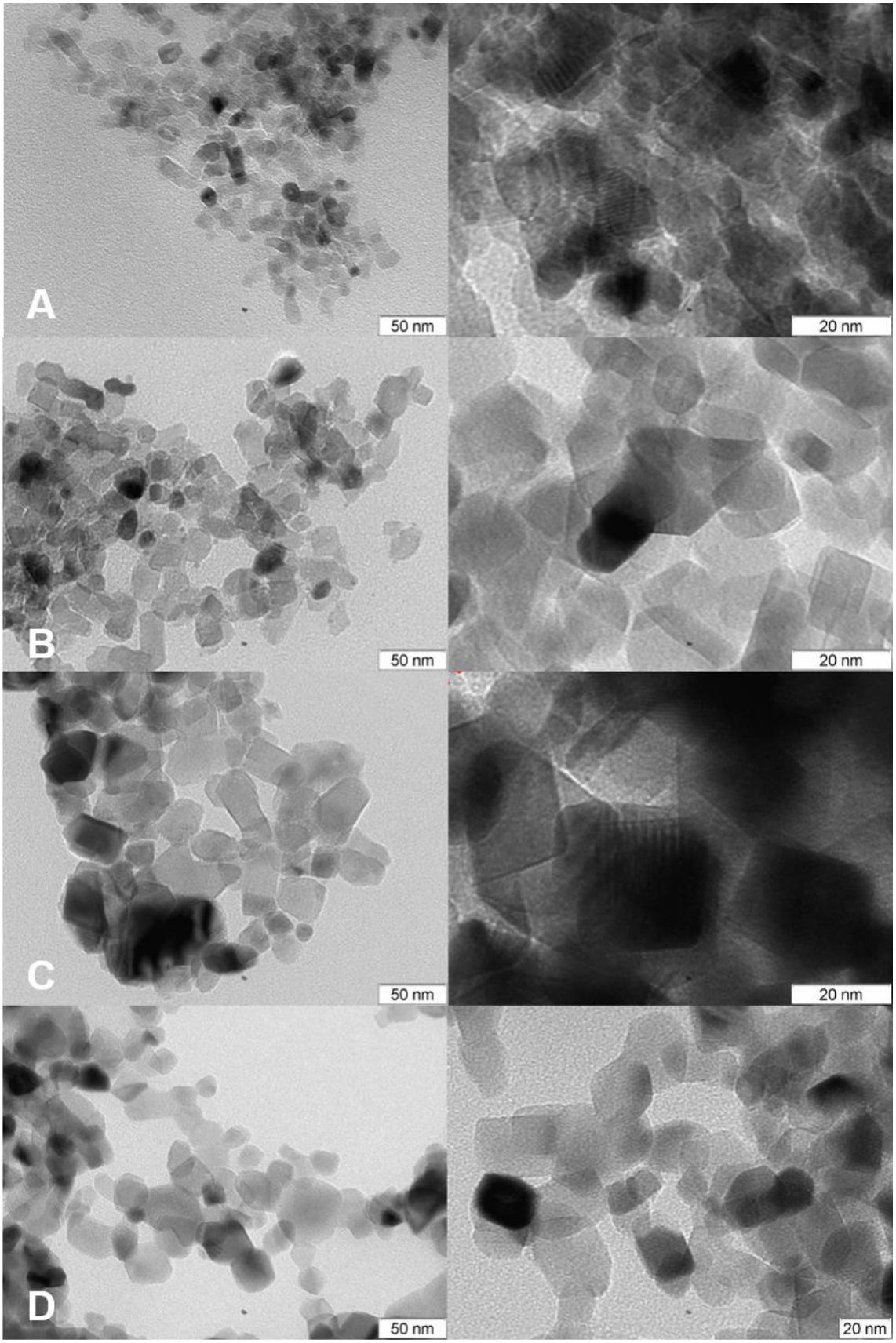

Figure 13. TEM images of the studied powders. **A-** TiO_2 synthesized powder calcined at 400ºC. **B-** TiO_2 synthesized powder calcined at 520ºC. **C-** TiO_2 synthesized powder calcined at 625ºC. **D-** Commercial anatase (Degussa P25).

3.1.3. Discussion

According to the results obtained from all the characterisations performed, a model for the formation and growth of TiO_2 nanoparticles can be suggested. The first proposal is relative to the chemical reaction that originates TiO_2. The first reaction that occurs is the loss of the four ethoxide groups and consequent formation of titanium hydroxide (Eq. 11). The second step is the diffusion of these molecules to the micelles surface and there the condensation process begins to occur (Eqs. 12 and 13). Therefore pluronic micelles play a more important role than initially expected. Not only they work as templates for the final mesoporous structure of TiO_2, but also serve as precursors for titanium dioxide's formation, hence making this type of precursor important since it guides and facilitates the structuring of the final form of the nanoparticles, working as a sort of catalyst for the reaction. The observed exponential growth and the final sizes of the particles obtained by the DLS measurements confirm this model. Another important conclusion is that temperature does not affect the final size of the nanoparticles. This is based on the fact that the final sizes achieved by the nanoparticles were basically the same (mean value around 13.4 nm), and changing the temperature only affected the time necessary to reach that final size. This probably occurs because increasing the temperature decreases the medium's viscosity and facilitates the molecules' diffusion to the micelles. Moreover, the k_{obs} values calculated lead to the conclusion that at lower temperatures gelation processes may start to occur (with a small contribution to the overall nanoparticle size). Performing concentration studies, varying TEOT and/or Pluronic P123 initial concentrations, would be helpful to further understand what is determining the nanoparticles' final size.

From the powder characterizations we found that calcination temperature influenced greatly the final powders' aspect. Increasing the calcining temperature affected, not only, the final size of the particles, as well as the pore volume and, consequently the surface area. All the powders produced were crystalline phases of titanium dioxide. Using temperatures from 400 to 520ºC led to the transformation from amorphous to anatase phase, whereas for temperatures as high as 625ºC anatase to rutile phase transition started to be promoted. Another important aspect is that calcining temperature does not affect the polydispersity of the particles' sizes, but the general final size. One major aspect that is important to clarify is that DLS measurements give notice of an average size value, and this does not imply that there is not dispersity in the sizes of the nanoparticles in the sample. Therefore, it is normal that there is not a direct relation of the results from the DLS measurements and the sizes revealed by the TEM analysis.

Based in the results obtained, the crystalline phase, size and more importantly surface area, and considering that one of the main objectives of this work is adsorbing dyes into the synthesized TiO_2, it was decided that all the synthesis, whether it was in powder or in film, were to be performed with calcinations at 400ºC, because this was the temperature that promoted the greater surface area and pore volume.

3.2. Synthetic and Natural Dyes

One major objective of this work was to use natural pigments from a biological source. Aware of the increasing necessity to develop sustainable technologies and to recycle compounds, we decided to use industrial biological waste materials as source for these natural pigments. Wine and olive oil waste residues were obtained from national producers from Reguengos, Alentejo and Passos de Pinho, Viseu, respectively, from the 2014 harvest. These production wastes were the source for the extracted pigments. The choice of these two industrial waste compounds was not random. Grapes and olives are known to be within the many fruits that owe their strong colour to anthocyanins (Figure 2A). Furthermore, anthocyanins are among the main families known to sensitize TiO_2 nanoparticles to use in solar energy conversion [35,36,40]. Being Portugal a country with a wine and olive oil tradition, and since the residues from olive oil production contain compounds pernicious to the environment [66], this choice seemed obvious.

A model compound was used throughout the entire study: 3',4',7-trihydroxyflavylium (Figure 2B). This flavylium is a synthetic analogue of anthocyanins and was synthesized and studied previously in the host laboratory [2,67,68]. Additionally this flavylium was proved to be a reasonable sensitizer for DSSCs, with final efficiency results of 1.22% [2].

Application in dye-sensitized solar cells could not be performed without studying in solution the dyes suggested in this work. Anthocyanins are responsible for a wide variety of colours seen in Nature and, sometimes, the same molecule can present different colours according to the surrounding environment. One such *stimuli* that can greatly affect the colour expressed by anthocyanins is pH. [10] Considering that anthocyanins and related compounds can equilibrate between flavylium cation (**AH^+**) (at low pH values) and quinoidal base (**A**) or hemiketal (**B**) species (at higher pH values) (Figure 14), the study of these different species network was performed by UV-Vis spectroscopy varying the pH of the solution. The best way to perform this type of study is to start with a solution at low pH, for example pH 1.0, to ensure the presence of the flavylium cation, and then add base gradually to promote the so-called direct pH jumps. Once this pH jump is promoted two parallel reactions are involved: deprotonation of the flavylium cation to form the quinoidal base (**A**) and/or hydration to lead to hemiketal formation (**B**). Since hemiketal formation only occurs from the hydration of the flavylium cation and not from the quinoidal base, these two reactions are competitive. Consequently, upon pH jump, **A** appears as a kinetic product, but since it is fairly unstable at equilibrium, it gradually disappears with time to form hemiketal through the flavylium cation. The hemiketal undergoes tautomerization which leads to the formation of *cis*-Chalcone (**Cc**), and finally (in a slower timescale) *cis*-chalcone isomerizes and gives the *trans*-Chalcone (**Ct**). The flavylium compounds thermodynamic equilibria can be considered equivalent to that of a single acid-base equilibrium between flavylium cation and a conjugate base (**CB**), where this last is defined as the sum of the concentrations of all the basic species in the network: **[CB]=[A]+[B]+[Cc]+[Ct]** (15), with approximately 10% of **A** and 90% of **Ct**. When the solution is equilibrated we have,

$$AH^+ + H_2O \overset{K'_a}{\rightleftharpoons} CB + H_3O^+ \quad (16)$$

thus calculating a

$K'_a = K_a + K_h + K_hK_t + K_hK_tK_i$ (17) [10,68,69].

In this study UV-Vis spectra were collected right after pH jump and after 24h, to allow thermodynamic equilibrium to be reached. This allowed the calculation of a pK_a value for the kinetic results, and a pK'_a for the thermodynamic equilibria results.

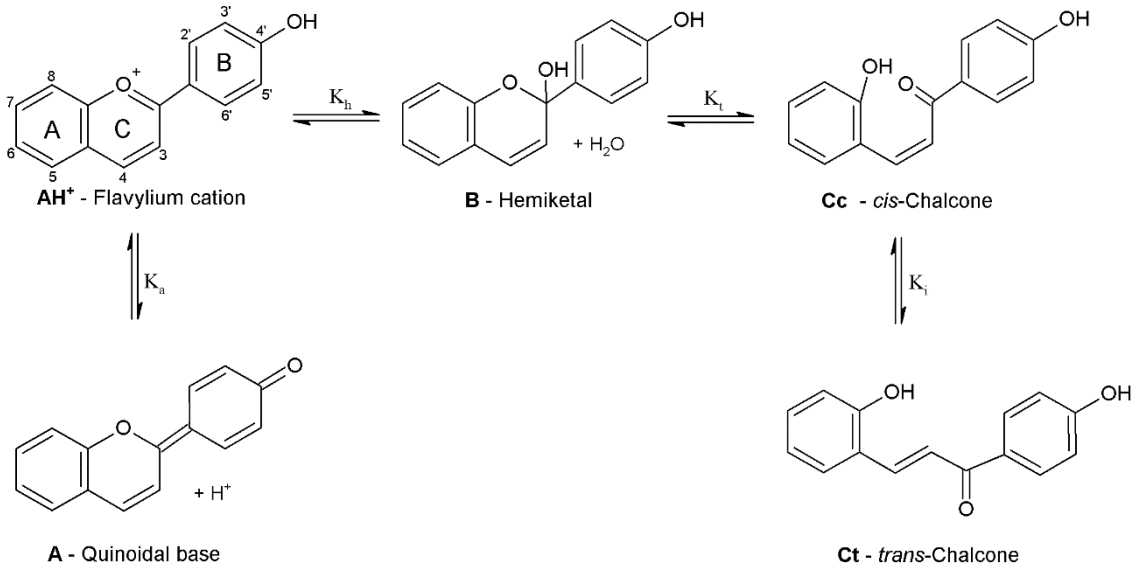

Figure 14. Flavylium network of chemical reactions.

Synthetic Dye - 3',4',7-trihydroxyflavylium

3',4',7-trihydroxyflavylium is a bioinspired structure synthesized to function as a quasi-natural biomimetic compound. These compounds are optimizations of what is found in Nature, where with some simple, non-toxic and environmentally safe procedures, components are introduced in the molecular structure or substituted, thus obtaining the desired characteristics.

Several studies, including pH studies, about this flavylium are reported [10,67–69] but since they were all performed in aqueous solutions, and our system uses pure ethanol as solvent, pH studies were performed to assess about the behaviour of this compound.

The initial pH of this study was ≈1.0 (initial pH was adjusted using HCl solution) to guarantee flavylium cation presence, and base (NaOH) was gradually added until a final pH of about 7 was reached. Figure 15A shows the UV-Vis spectra obtained from this study. About 24h later, after

the solution had equilibrated, UV-Vis spectra were again collected (Figure 15B) and calculated, respectively, the pK_a and pK'_a of the system in solution.

Briefly, assuming, as already said, a single acid-base equilibrium, we have

$$AH^+ + 2\,H_2O \overset{K'_a}{\rightleftharpoons} CB + H_3O^+ \qquad (18)$$

where $K'_a = \frac{[CB]\times[H^+]}{[AH^+]}$ (19),

from this equation we have

$[CB] = \frac{K'_a}{[H^+]+K'_a} \times [AH^+]_0$ (20) and

$[AH^+] = \frac{[H^+]}{[H^+]+K'_a} \times [AH^+]_0$ (21).

Knowing that the total Absorbance of the sample is given by

$Abs^M = \varepsilon^{CB} \times [CB] + \varepsilon^{AH^+} \times [AH^+]$ (22),

substituting with equations 20 and 21, and simplifying we have the final equation to adjust our data

$$Abs^M = \frac{Abs^{CB}\times 10^{-pK'a} + Abs^{AH^+}\times 10^{-pH}}{10^{-pK'a} + 10^{-pH}} \qquad (23).$$

As is evident in Figure 15A with the increase in the pH of the solution came a decrease of the peak at 489 nm (correspondent to the flavylium cation) and an increase of a peak at 380 nm (correspondent to the chalcone formation) as a consequence of basic species formation, resulting in an isosbestic point at around 410 nm. Accordingly, from the absorbance results observed at 489 nm as a consequence of pH increase, and applying equation 23, a pK_a=3.04 for the reaction after pH jump was calculated. Figure 15B portraits similar results after equilibrium, with the decrease of the peak at 489 nm and consequent appearance of the peak at 380 nm, indicating the formation of **Ct**. As is noticeable the final spectra are different from those in Figure 15A. In Figure 15A there is evidence of a slight red-shift, starting at pH≈4.0, corresponding to the formation of the only other coloured specie, the quinoidal base. Which means that at pH≈4.0 the kinetic product, quinoidal base, starts to appear. Since this is a kinetic product, and as explained before, after thermodynamic equilibria is reached the predominant basic species is no longer the quinoidal base, this red-shift is absent in Figure 15B. Since thermodynamic equilibrium was reached, this means that the quinoidal base formed after pH jump reconverted to cation flavylium and was then converted in hemiketal and the other basic species this compound can convert into. Being so, the increase of the maximum absorbance observed at 380 nm (from approximately 0.3 in Figure 15A to approximately 0.6 in Figure 15B) is due to quinoidal base disappearance and

appearance of the other basic forms. A pK'$_a$=1.98 for the equilibrated reaction is calculated. Both the maximum wavelength and pK$_a$ and pK'$_a$ values calculated are different from what is reported [67,68]. The reported λ_{max} (flavylium cation) is at approximately 469nm, while the λ_{max} for the basic species after equilibrium is around 380 nm as well [67,68]. The reported pK$_a$=4.1 and pK'$_a$=3.1 are also different [67,68] following the same "pattern" since the pK'$_a$ value is smaller than the pK$_a$. These differences are probably due to solvatochromic effects, since the presented experiments were performed in pure ethanol, and the reported results are from aqueous solutions.

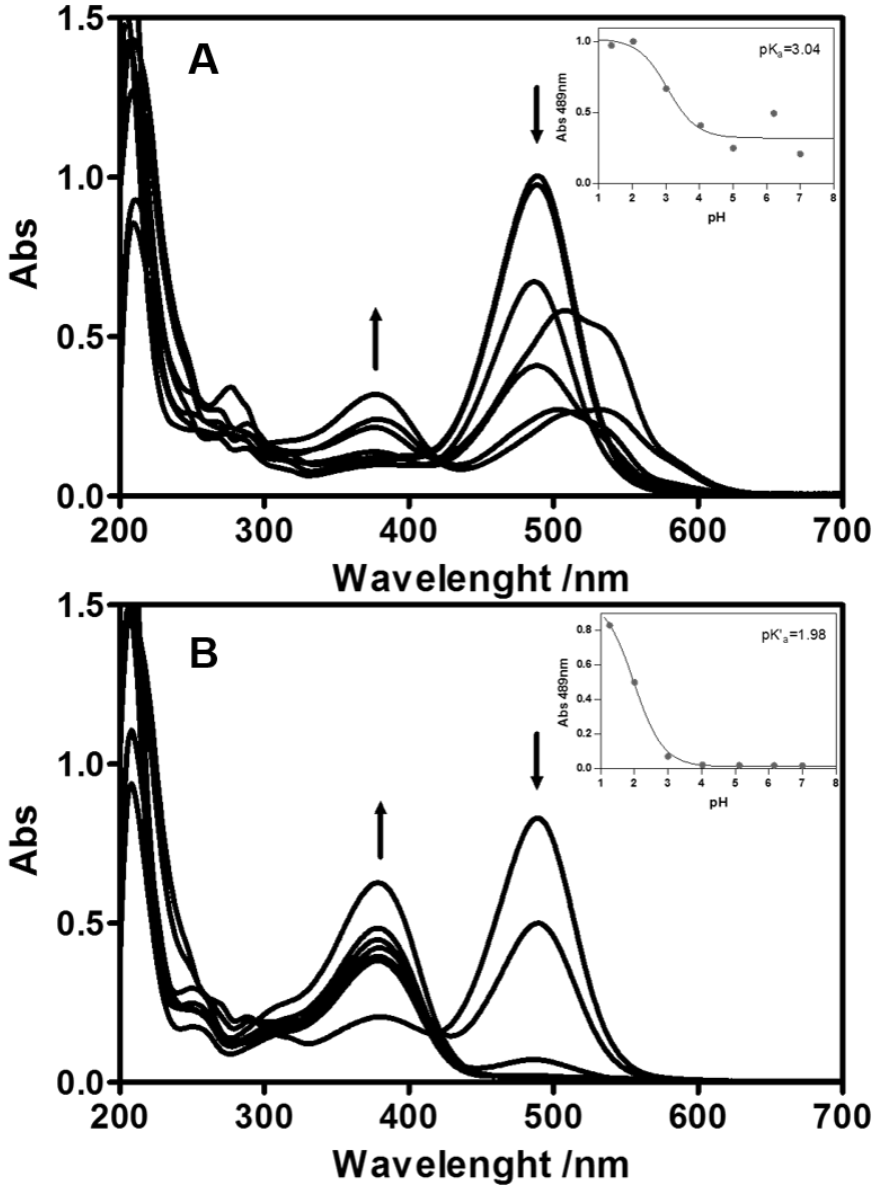

Figure 15. UV-Vis spectral variations occurring upon a pH jump from a stock solution of 3',4',7-trihydroxyflavylium, in ethanol, at pH 1.0 to higher pH values (adjusted with NaOH). **A-** Spectra recorded immediately after the pH jump (<1 min after adding base). **B –** Spectra recorded after thermodynamic equilibrium being reached (≈24h). Inserts: fittings (——) of the absorbance values (●) at the specified wavelengths. Plot of the dependence of the Abs values registered at 489 nm with pH increase: pK$_a$= 3.04 and pK'$_a$=1.98.

Natural Dyes – Wine and olive oil waste

Anthocyanins belong to the flavonoid group and are a family of water-soluble chemical compounds that occur naturally in plants. Grapes and olives are among the many fruits and flowers that owe their colour to anthocyanins. The core of anthocyanins is a 2-phenyl-1-benzopyrilium (flavylium), which consists of an aromatic ring (A) bonded to a heterocyclic ring (C) containing an oxygen atom which is then linked by a C-C bond to a third aromatic ring (B) (Figure 14). Anthocyanins have pendant sugars. The variety of possible dye colours present in Nature is due to the presence and differences in the number of hydroxyl and/or methoxyl groups in the molecule, the nature and number of sugar moiety attached to the phenolic units and the nature and number of aromatic or aliphatic acids attached to the sugar moieties. The number of hydroxyl and methoxyl groups is what determines the intensity, type (concerning the absorption wavelength) and stability of anthocyanins' colour [40].

Between the various pigments found in grapes and olives, cyanidin-3-glucoside, malvidin-3-*O*-rutinoside and malvidin-3-*O*-coumaroylglucoside [36,40,45,46] are known to be responsible for the purple colour of grapes, and cyanidin-3-*O*-glucoside and cyanidin-3-*O*-rutinoside [47–51] are pointed as being responsible for the black colour of olives. All these molecules are anthocyanins normally found in various natural fruits.

To perform a pH study of these natural pigments the same procedure (as done for the synthetic flavylium) was followed. Although in contrast with the synthetic flavylium, which was in the form of a powder, these pigments had to be extracted from the biological waste samples. This extraction process was performed in pure ethanol, since it is biocompatible and environmentally safe, and since water revealed to be a poor extraction solvent. The as-sent waste products were placed in a solution of acidified ethanol in the dark under stirring at approximately 40ºC, for 3h. The resultant solutions were purple, from the wine waste, and yellow, from the olive oil waste. Since the extraction process was performed on the as-sent samples it also included the skin and seeds of the fruits. Being so, after the extraction process was finished, the solutions were filtered. An UV-Vis study was performed with these solutions starting at pH≈1.0 and adding base gradually. The UV-Vis spectra were collected after pH jump and at thermodynamic equilibrium.

Figure 16 shows the results of the pigment from the wine waste extraction. After pH jump (Figure 16A) and increasing the pH of the solution, there is a clear decrease of the peak at 546 nm with no clear appearance of a peak correspondent either to the quinoidal base (red shifted) or from the hemiketal formation (in the UV region). This absence of peaks correspondent to the basic species does not mean that the compounds present in solution are not anthocyanins. Since these solutions are the result of an extraction from a natural source, specific anthocyanin extraction cannot be assured, thus the assumption of the presence of other compounds in solution has to be made (as can be seen by the peak at around 660 nm, probably corresponding to chlorophylls,

which, in this case, were not affected by pH alterations). The most probable explanation for the absence of peaks corresponding to the basic species is that the mixture under study precipitated. At pH≈6.0 the solution became more turbid and small precipitates started to form when adding more base and changing to higher pH values. An important aspect to keep in mind is that the pigments' source is not a sample of fresh grapes, but the result of wine production. When producing wine, fermentation processes occur, with the consequent formation of the pyruvic acid adducts of the pendant sugar of anthocyanins (e.g. cyanidin-3-glucoside-pyruvic acid adduct and malvidin-3-glucoside-pyruvic acid adduct) [45]. Given this, and adding to the fact that these flavylium compounds are prone to form complexes with other molecules (it is a strategy used in Nature to obtain different colours) [10], it is quite probable that the basic species had precipitated because of complexation with other molecules. Despite the absence of the expected isosbestic point, a pK_a=3.17 value was calculated for this reaction from the spectra run immediately after each pH jump. Figure 16B represents the results at thermodynamic equilibrium. The UV-Vis spectra are almost identic and so is the pK'_a=3.07 calculated. This result means that the equilibrium composition is closer to the initial composition than what was observed in the synthetic flavylium. This means that in Figure 16A, right after pH jump, the reaction is so fast that the spectra collected were probably those of the thermodynamic equilibrium and not from the kinetic products. Therefore, both the values calculated are correspondent to the pK'_a of the reaction, which means the pK_a calculated (present in Figure 16A) is actually a pK'a value.

Figure 17 presents the results of the pigment extracted from the olive oil waste. Opposite to what was expected, the spectra show no signs of anthocyanin presence. A pH jump, from pH 1.0 to 8.0, was performed and no change of intensity, or peak shift or disappearance was observed. Since when producing olive oil only chlorophylls and carotenoids (which are fat-soluble) are transferred to the virgin olive oil, resulting in its characteristic yellow colour, the production's waste should be loaded with anthocyanins. [48] Given the colour of the solution resulting from the extraction process (yellow as opposed to the black colour expected) and the spectra obtained, probably the pigments extracted from the biological waste are carotenoids and/or chlorophylls, and not the desired anthocyanins. Apparently, the acidified ethanol was not a strong enough solvent to perform an efficient extraction of the anthocyanins present in the olive oil waste. Further studies would be needed to confirm this hypothesis carrying out extractions with other solvents. Since the spectra did not change upon pH jumps, a pK_a value could not be determined.

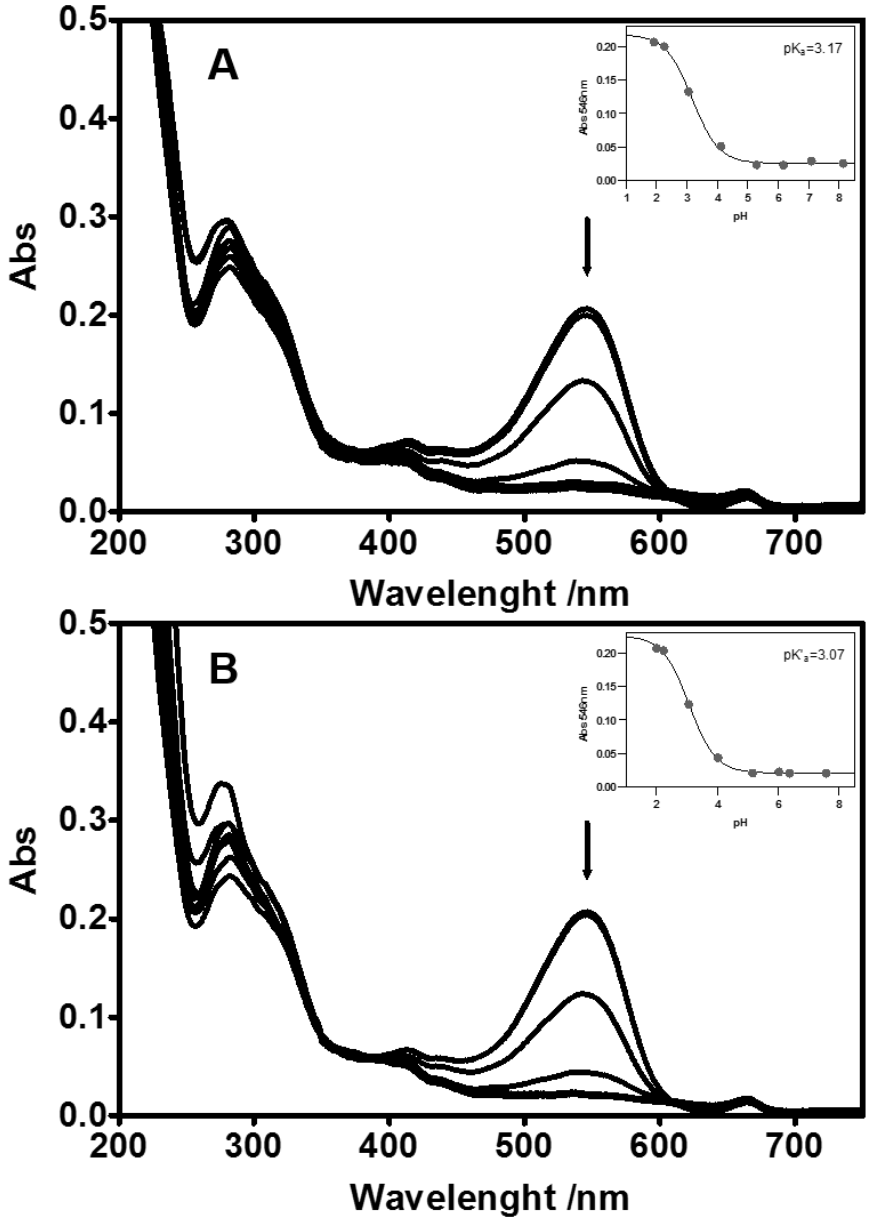

Figure 16. UV-Vis spectral variations occurring upon a pH jump from a stock solution of the pigment extracted from the wine waste, in ethanol, at pH 1.0 to higher pH values (adjusted with NaOH). **A-** Spectra recorded immediately after the pH jump (<1 min after adding base). **B –** Spectra recorded after thermodynamic equilibrium being reached (≈24h). Inserts: fittings (——) of the absorbance values (●) at the specified wavelengths. Plot of the dependence of the Abs values registered at 546 nm with pH increase: pK_a= 3.17 and pK'_a=3.07.

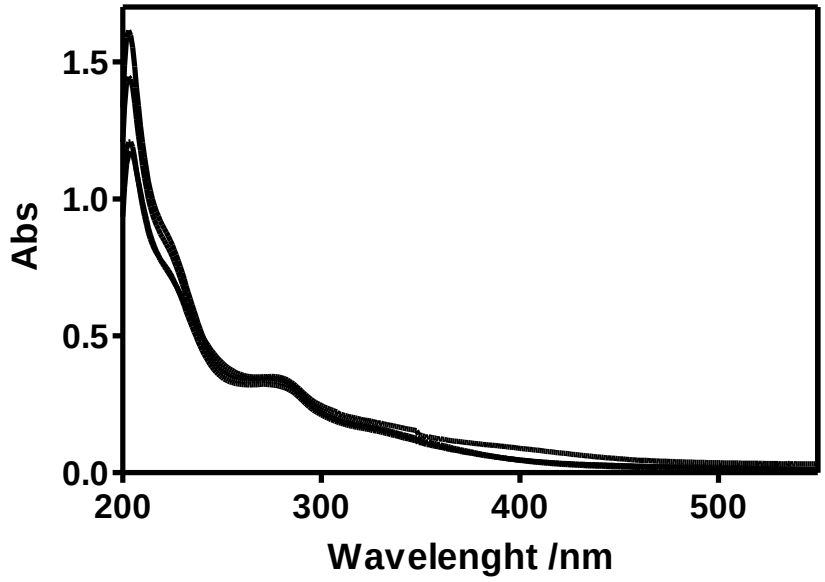

Figure 17. UV-Vis spectral variations occurring upon a pH jump from a stock solution of the pigment extracted from the olive oil waste, in ethanol, at pH 1.0 to higher pH values (adjusted with NaOH). Spectra recorded immediately after the pH jump (<1 min after adding base).

Dyes' adsorption into TiO_2

The final intention of this study is to perform dye adsorption into the synthesized TiO_2 mesoporous structure. Hence the studies performed were an optimization process to choose the pH of the solution for the adsorption tests. Table 3 summarizes the results obtained and the pH chosen to perform dye adsorption.

Table 3. Summary of the pK_a and pK'_a values calculated from the pH study followed by UV-Vis spectroscopy.

	pK_a	pK'_a	Optimum pH
3',4',7-trihydroxyflavylium	3.04	1.98	1.0
Wine waste	3.17	3.07	2.0
Olive oil waste	-	-	2.0

Considering the approximation to a single acid-base equilibrium, K_a and K'_a values, are acidity constants that give the information about proton-donating strength of the correspondent acid. Which means that these values give an idea of the pH range for stability of the flavylium cation, respectively, immediately upon a pH jump and after the equilibrium is established. The values of pK'_a or pK_a allow thus an adequate choice of solution pH at which the adsorption step should be carried out. Since these values represent the pH at which equilibrium has been reached in the acid-base system, thus implying that proton loss has already occured, we chose to work with

solutions with pH's approximately 1.0 value inferior to the pK'_a values calculated. This way, the predominant specie in solution is the flavylium cation (**AH^+**) but still the solution is at a pH value that is sufficiently close of the pH were proton loss occurs, thus facilitating the adsorption of the dye molecules into the TiO_2. Figure 18 shows a schematic representation of how the 3',4',7-trihydroxyflavylium is expected to adsorb into TiO_2. Loss of protons in the 3' and 4' positions allow the synthetic dye to establish bonds with TiO_2. The same behaviour is expected from the anthocyanins from the natural pigments. Both cyanidin and malvidin (independently of the pendant sugars) have available –OH groups able to chelate with TiO_2 after deprotonation. Therefore, to perform the adsorption step the solutions were prepared at pH≈1.0 for the synthetic flavylium and at pH≈2.0 for the wine and olive oil waste pigments. For the olive oil waste pigment's solution the pH choice was based in pragmatic concerns, since the pK'_a value was not possible to be determined.

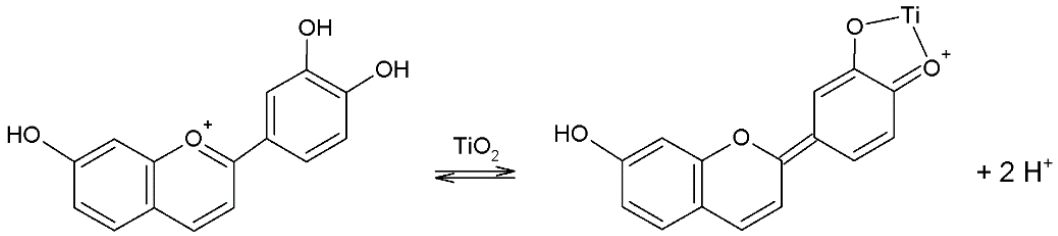

Figure 18. Schematic representation of the adsorption of 3',4',7-trihydroxyflavylium into the TiO_2.

Having defined the optimum pH for each solution, a small portion of the synthesized TiO_2 powder calcined at 400ºC (≈100 mg) was put in each of the dye solutions (≈10 mL) and left to react in the dark under stirring for about 1 hour. The final powders collected are presented in Figure 19. As is shown in the picture all the TiO_2 samples adsorbed dye as expected and became the colour of the respective sensitizer's solution. Sample A is relative to the synthetic flavylium and had a dark red colour, sample B is relative to the extract from the wine waste solution and had a purple colour and finally, sample C is relative to the extract from the olive oil solution and had a yellow colour.

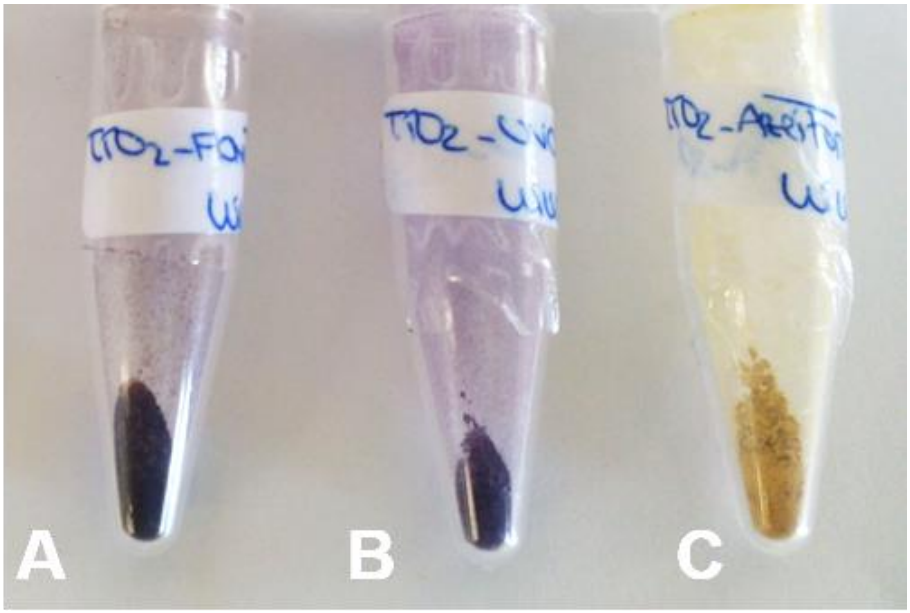

Figure 19. A- 3',4',7-trihydroxyflavylium adsorbed in the synthesized TiO_2 powder calcined at 400ºC. **B-** Dye extracted from the wine waste adsorbed in the synthesized TiO_2 powder calcined at 400ºC. **C-** Dye extracted from the olive oil waste adsorbed in the synthesized TiO_2 powder calcined at 400ºC.

These results proved that the TiO_2 nanoparticles synthesized can adsorb compounds onto their pores. The coloured powder samples were then analysed by DSC-TGA technique. Figures 20 A, B and C are referent to the flavylium, wine waste and olive oil waste samples, respectively. All the samples present similar results with the TGA line presenting a biphasic behaviour. This type of descending curve is generally associated with desorption and/or decomposition processes. The first weight loss visible in the TGA curve (for the three samples) is associated with water evaporation. The second, and more evident weight loss is due to dye decomposition and desorption from the TiO_2 powder. This result is confirmed by the fact that in the end of the measurement the powders returned to their original white colour, losing all the colour gained through dye adsorption. Since all the colour was lost, knowing how much of the total weight loss is due to water evaporation and assuming that only dye is responsible for the second visible weight loss (with no contribution from remaining organic matter present in the pores, as seen in Figure 11), the percentage of weight loss from the powder is equivalent to the amount of dye adsorbed into the TiO_2 nanoparticles. Hence approximately 4.6 (Figure 20A), 4.2 (Figure 20B) and 5.5% (Figure 20C) of the samples prepared in the study were dye from the adsorption process. The DSC curves do not display any significant results. (The peak seen in the DSC curve of Figure 20A is probably due to an error. This measurement would have to be repeated.)

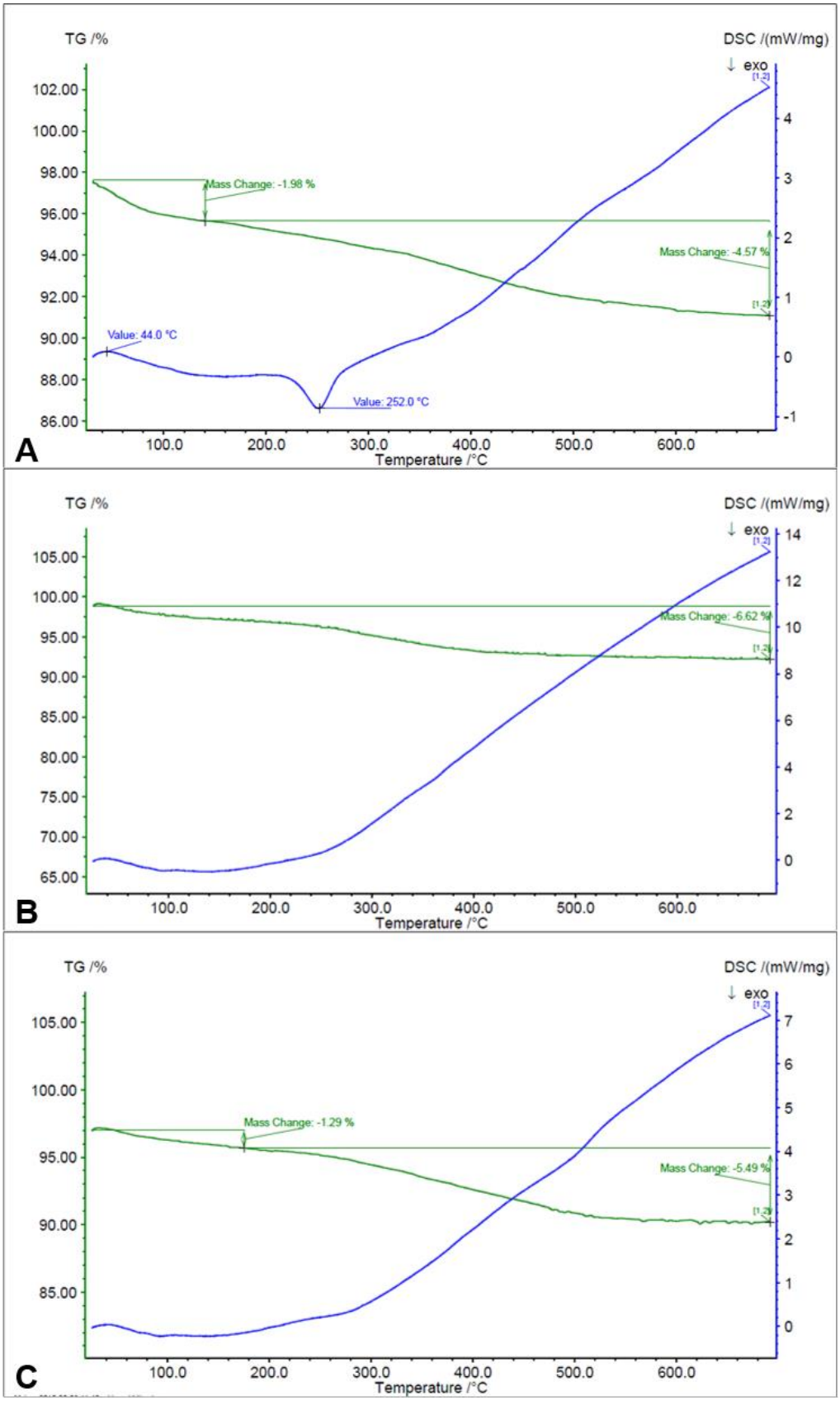

Figure 20. DSC (blue line) and TGA (green line) analysis of the synthetic flavylium 3',4',7-trihydroxyflavylium (A), the dye extracted from the grape waste (B) and the dye extracted from the olive waste (C) adsorbed in the synthesized powder calcined at 400ºC. Scan rate equal to 10ºC/min.

3.3. Photodegradation of Biological Waste Compounds using TiO_2 as a Catalyst

For the past years one major concern has been the increasing necessity to elaborate ways of degrading compounds that could be pernicious to the environment. Several methods have been developed throughout the last decades, one of which is Photocatalysis. Photocatalysis is a photodegradation process which is basically the inverse of photosynthesis, meaning that, instead of using light as a source of energy to produce O_2 and carbohydrates (Eq. 8), in photodegradation light is used to promote the degradation of compounds to their simplest inorganic form, e.g. CO_2 and H_2O. Titanium dioxide is a well-known and widely explored catalyst to this photodegradation reactions. [53] However, and as was explained before, its photocatalytic activity remains insufficient for practical application. Due to its wide band-gap, TiO_2 can only absorb light in the UV region. Since only less than 5% of the solar light that reaches the Earth is in the UV region, this process is limited right from the beginning, thus not allowing an effective use of sunlight to drive the reaction when pure TiO_2 is used as a catalyst. To overcome this drawback a strategy similar to what happens in DSSCs is usually applied. Extending the photo-response of TiO_2 to the visible region can be done by means of dye-sensitization of TiO_2 (adsorbing a dye into the TiO_2), thus making visible light harvesting possible. In this strategy, and as happens in DSSCs, TiO_2 has the 'charge-carrier' function. The dye molecules act as *antennae* to absorb the light energy into the degradation system. The principle of operation is the same: photoexcitation of the dye (Eq. 1) results in the injection of an electron into the conduction band of the semiconductor (Eq. 2a). In the presence of O_2 the existing pollutants, or the adsorbed dye itself (in case this is the target), can be oxidized to CO_2, H_2O and other products. Organic compounds, as well as dye pollutants from the textile industry, are sources of environmental contamination and are, therefore, potential targets for this type of photocatalysis. [55,60]

In this chapter a system was developed with the objective of degrading the dye extracted from the wine production's waste, using the synthesized TiO_2 as catalyst, and by irradiating the system with visible light. By adsorbing the dye into the TiO_2, this later only has the function of charge-carrier, thus attributing the light-harvesting role to the target dye (thus acting as the so called *antennae*). The objective of this system is to prove the concept presented above.

This work was developed using as base the methodology developed in [4], which will be explained next. To develop the desired system the first step was to adsorb the dye into the TiO_2. As proved in the previous chapter, the dye extracted from the wine waste can be adsorbed into TiO_2, but this reaction had to be optimized to understand how much time was needed to saturate the TiO_2 with dye (to improve the efficiency of the system, by degrading as much dye, at a time, as possible). To do so 250 mg of the synthesized TiO_2 powder (calcined at 400ºC) were added to a solution of 10 mL of the grape dye extracted and 20 mL of ethanol (pH≈2.0). This solution was placed in the dark under vigorous stirring and the reaction was followed for 3 hours. Small aliquots of the solution (≈2 mL) were taken at predetermined time intervals, centrifuged and the

supernatant was analysed by UV-Vis spectrophotometry. The results obtained are shown in Figure 21. A decrease of the absorbance measured at approximately 549 nm is seen. Since this peak is associated with the anthocyanins present in the wine waste, the disappearance of this peak is due to dye adsorption (in the flavylium cation form) into the TiO_2 pores. It is also noticeable the appearance of a peak at about 610 nm, correspondent to the quinoidal base formation. This is a rather interesting result since when performing the pH studies no basic specie of the anthocyanins was visible. But in the presence of TiO_2, quinoidal base formation occurs, since for some anthocyanins (such as cyanidin-3-glucoside) upon adsorption onto TiO_2 the equilibrium between the forms is believed to shift towards the quinoidal form. [35] This disappearance of the acidic species with the consequent appearance of the basic one, gave rise to an isosbestic point around 590 nm. Another interesting aspect is the presence, once more, of the peak around 660 nm, which means that the extraction process is reproducible (since the same species are present) and that the compound responsible for that peak is not adsorbed onto/ affected by TiO_2 since no peak alterations are noticeable. This study allowed to understand the kinetics of dye adsorption as well. Figure 21 (Insert) shows the decrease of the absorbance measured at 549 nm in function of the time of reaction. This peak decrease is associated with the adsorption of the dye onto the TiO_2. After about 60 minutes of reaction there is a stabilization of the absorbance measured, which indicates that an equilibrium was reached.

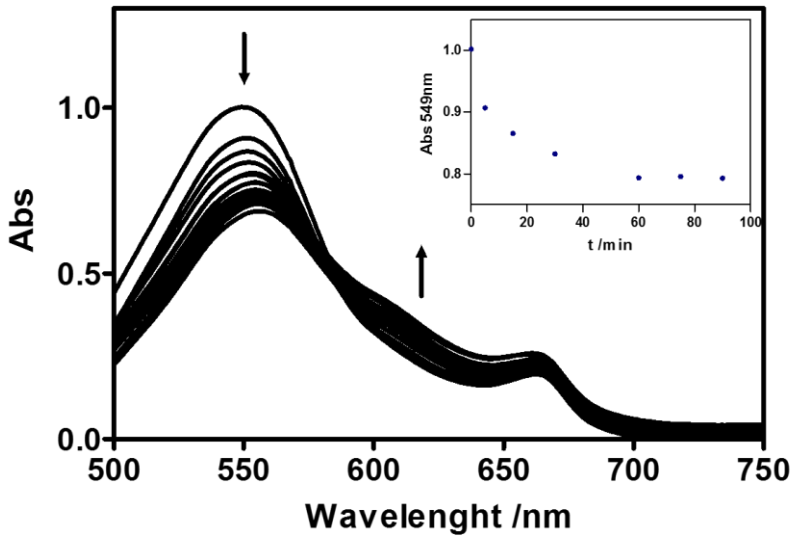

Figure 21. UV-Vis spectra obtained from the adsorption of the pigments from the wine waste into the synthesized TiO_2. Insert: Plot Abs 549 nm vs. time.

After defining the time necessary to the dye adsorption step, and since the photodegradation study would occur in water, a “Leaching-out” test was performed to see if leaching of the dye into water occurred. This test was important to later confirm that the loss of colour from the powder (after the irradiation of the sample) was really a consequence of the biological dye’s degradation,

and not because desorption of the dye from the pores to the water (leaching-out) was occurring. To perform the leaching-out test 150 mg of the coloured powder obtained were added to 20 mL of milli-pore water. The procedure was the same: in the dark under stirring and the reaction was followed during 2 hours, collecting aliquots, centrifuging and analysing the supernatant by UV-Vis spectrophotometry. Figure 22 shows the results obtained. As is observed there are no evidences of any anthocyanin desorption taking place, since there is no peak appearance around 550 nm. Since there is no peak appearance anywhere in the spectra, it indicates that there is no degradation process taking place. This results indicate that the anthocyanins present in the biological dye have a greater affinity to the titanium dioxide pores than to water.

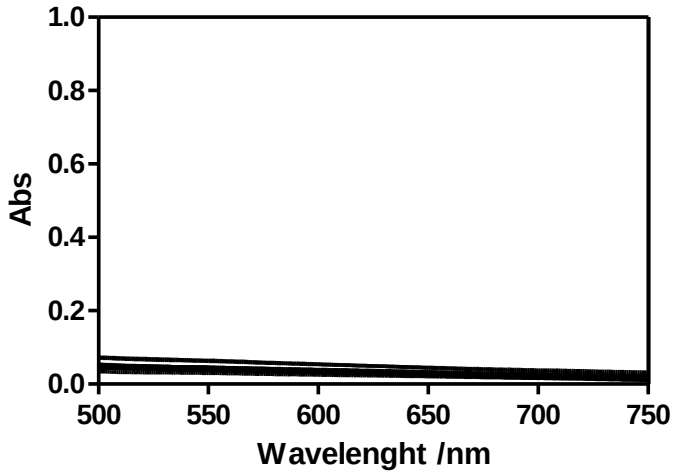

Figure 22. UV-Vis spectra obtained from the 'Leaching-out' study performed placing the TiO_2 powder with adsorbed pigment extracted from the wine waste in milli-pore water.

Since no leaching of the dye occurred it was possible to perform the photodegradation test as planned. To perform this photodegradation test, the irradiation process was performed adding 30 mg of the coloured powder (TiO_2 with the dye extracted from the wine waste adsorbed) to 6 mL of milli-pore water and irradiating the sample at 546 nm with a Xe/ Hg lamp (300W) under stirring, for 5 hours. The powder was then collected, dried and analysed. The powders obtained from this study are shown in Figure 23. Sample A corresponds to the powder collected after the adsorption study, a purple powder resulting from the adsorption of the dye from the wine waste onto the titanium dioxide. Sample B is a portion of the same powder after the photodegradation process. It is quite obvious the difference in colour from sample A to B. Sample B lacks colour when compared to sample A, meaning that the photodegradation reaction took place, and that we were able to degrade the anthocyanins adsorbed with visible light stimulation, and using TiO_2 as a catalyst.

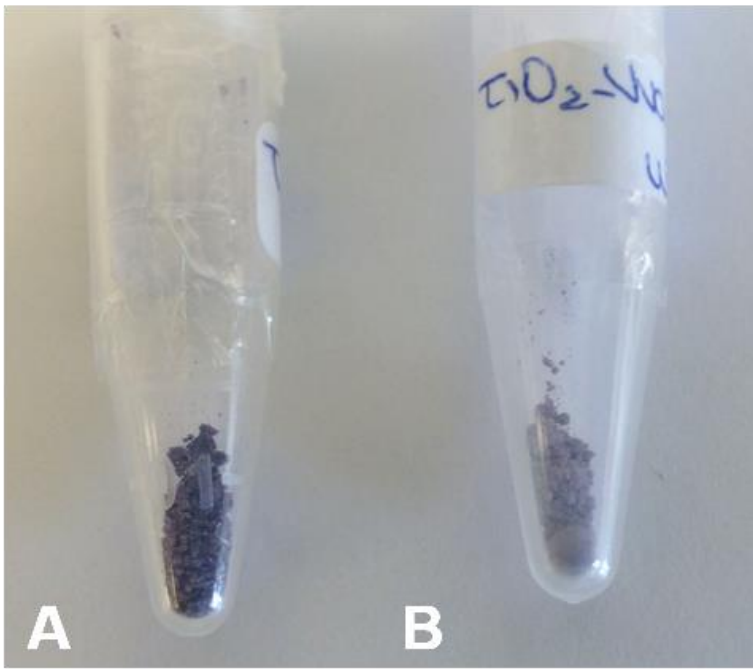

Figure 23. A- Titanium dioxide powder synthesized and calcined at 400ºC after adsorption of the pigments from the wine waste. **B-** Titanium dioxide powder synthesized and calcined at 400ºC with pigments from the wine waste after irradiation at 546 nm with a Xe/Hg lamp, under stirring, for 5 hours.

Reflectance spectroscopy was used to study the powders produced in this chapter. Figure 24 shows the results obtained. Three spectra are shown: the dark purple is correspondent to sample A (Figure 23) which is the powder resulting from the adsorption step, the light purple is correspondent to sample B (Figure 23) which is the powder resultant from the photodegradation step and the grey, which is the spectra of the TiO_2 powder synthesized and calcined at 400ºC. Looking at these spectra there is a clear evidence of loss of colour in sample B, confirmed by the decrease of the peak at approximately 580 nm, which supports the visual results from Figure 23. Furthermore, comparing the TiO_2 spectrum with those from the coloured species provides clear evidence of dye adsorption, since no peak is observed in the visible region of the TiO_2 spectrum, whereas a peak at approximately 580 nm is seen in both the coloured samples. These results provide strong evidence of the occurrence of photodegradation of the dye extracted from the wine waste adsorbed in the TiO_2, thus proving that this system works: TiO_2 can adsorb the dye, the dye adsorbed can harvest light in the visible region and efficiently inject the electrons into the conduction band of TiO_2, thus allowing its own degradation. This result fulfils the proof of concept purpose, providing evidence that this type of degradation could be applied on dye pollutants from the textile industry for example, and could possibly be applied to degrade the pernicious compounds found in the waste from olive oil production.

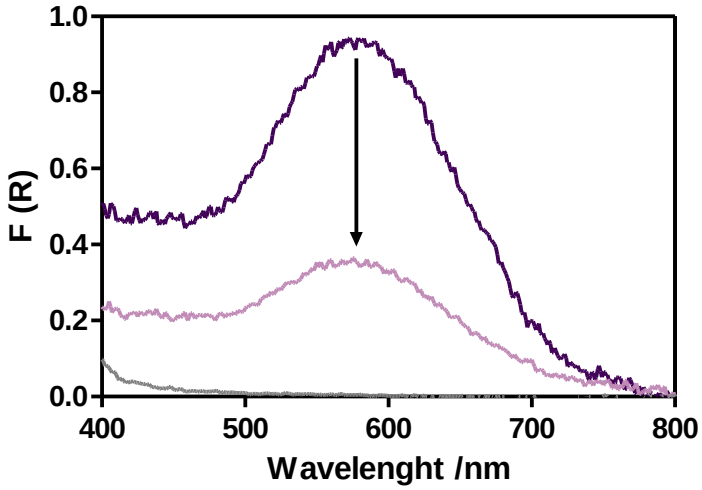

Figure 24. Reflectance spectra from: Titanium dioxide powder synthesized and calcined at 400ºC after adsorption of the pigments from the wine waste (—); Titanium dioxide powder synthesized and calcined at 400ºC with pigments from the wine waste after irradiation at 546 nm with a Xe/Hg lamp, under stirring, for 5 hours (—); Titanium dioxide powder synthesized and calcined at 400ºC (—).

The two powders (from Figure 23) were then subjected to DSC-TGA analysis to evaluate what was remaining adsorbed in the pores. Figure 25 shows the results for sample A (relative to Figure 23A), the powder after the adsorption step. The first mass decrease of about 2.6% is probably associated with water loss. For temperatures higher than 100ºC an increase of mass loss is visible, resulting in a decrease of about 2.5% in the overall weight, due to dye degradation, once more supported by the fact that in the end of the study the powder returned to its original white colour. Besides the disparity in the initial weight loss, probably because this sample was less dried than the one in the previous chapter, the DSC curve behaviour is quite similar, with no major peaks, and the TGA line, after that abrupt weight loss in the beginning, shows a similar behaviour as well (comparison with Figure 20B).

Figure 26 shows the results for sample B (relative to Figure 23B), the powder resultant from the photodegradation study. The most obvious differences in the DSC curve is the appearance of peaks, both endo- and exothermic, neither of which with much significance. These peaks are probably associated with loss of photodegradation compounds. The first endothermic peak, seen at 43.8ºC, is associated with an increase of weight of about 1.4% in the TGA curve, which is probably due to gas absorption from the sample. The overall weight loss due to the photodegradation products for sample B (Figure 26) is 7%, whereas for sample A (Figure 25) the overall mass loss due to dye disappearance is of about 2.5%. This increase in the total weight loss is not due to increased dye adsorption from sample B, but because of the existence in this sample of products from the photodegradation reaction. These results give evidence of the mineralization of the anthocyanins into CO_3^{2-}, since the carbons that were previously linked with each other (Figure 2A), are now linked with three oxygen atoms. An example is given for better understanding of this question. Taking the cyanidin-3-glucoside molecule $C_{20}O_{11}H_{20}$ (Figure 2A),

if this molecule completely mineralized to CO_3^{2-} in the presence of oxygen, the following reaction would take place:

$$C_{20}O_{11}H_{20} \rightarrow 20\ CO_3^{2-} + 10\ H_2O \qquad (24)$$

Cyanidin-3-glucoside has a molecular weight (MW) of ≈436 $g.mol^{-1}$, its degradation would lead to products with a total MW of ≈1200 $g.mol^{-1}$, which represents about 2.7 times more mass. From sample A (mass loss of ≈2.5%, Figure 25) to sample B (mass loss of ≈7%, Figure 26), there was an increase of mass loss of ≈2.8, which corroborates the fact that total mineralization of the anthocyanins responsible for the purple colour seen in sample A occurred. This is what is thought to be happening in the photodegraded sample, thus the increase of mass loss is not due to increased dye adsorption, but from the occurrence of photodegradation of the dye adsorbed (in sample B).

This type of TGA line is associated with desorption and decomposition processes, and since the final samples were, again, completely white (the TiO_2 original colour) the weight losses are associated with the total decomposition of the adsorbed compounds giving an idea of how much dye and photodegradation products were adsorbed in the powders.

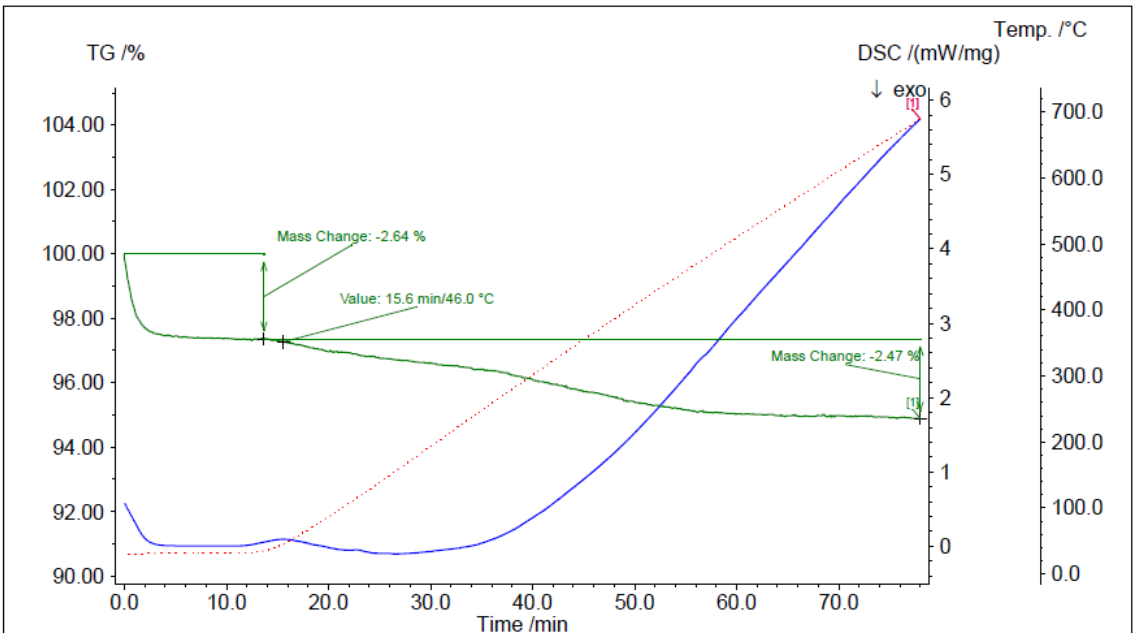

Figure 25. DSC (blue line) and TGA (green line) analysis the TiO_2 synthesized powder calcined at 400ºC with the dye extracted from the wine waste adsorbed in. Scan rate equal to 10ºC/min.

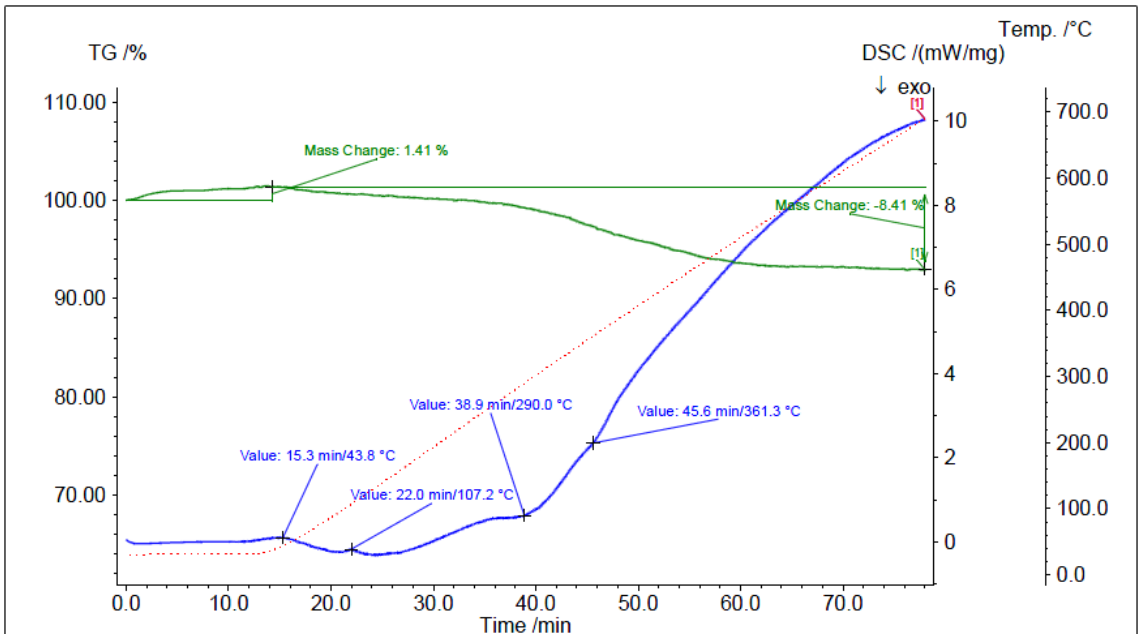

Figure 26. DSC (blue line) and TGA (green line) analysis the TiO_2 synthesized powder calcined at 400ºC with the dye extracted from the wine waste adsorbed in, after 5 hours of irradiation with a Xe/Hg lamp, at 546 nm. Scan rate equal to 10ºC/min.

3.4. Application in Photochemical Devices

There is a wide range of applications for mesoporous TiO_2 in the field of chemical devices. We explored the possible application in photochemical devices (Dye-Sensitized Solar Cells), based on the photovoltaic effect, using an n-type semiconductor (TiO_2) dye-sensitized by natural anthocyanins from wine and olive oil productions' waste and a synthetic analogue of anthocyanins (3',4',7-trihydroxyflavylium).

In a dye-sensitized solar cell the objective is, ultimately, the production of energy, hence electric current, from solar light. In a DSSC there is electronic conduction, charge carried by electrons, and ionic conduction, charge carried by ions. Since production of electric current depends on the electronic conduction performed by the semiconductor, it plays a vital role in DSSCs. The mesoporous film has to carry the electrons injected by the excited dye, to the FTO glass for the production of electric current outside the cell. This is why calcining/sintering processes are of major importance. TiO_2 nanoparticles *per se* are insulators, which means that they have such a high resistance, they do not conduct electricity (Figure 27A). By calcining/sintering compounds we promote percolation, and therefore, the production of a semiconductor. In an intrinsic semiconductor an empty conduction band lies close in energy to a full valence band, as a result, electrons can be excited from the valence into the conduction band, thus carrying current. To enhance this ability one can either add electrons to the conduction band or remove electrons from the valence band. This can be performed by chemically doping the material producing an extrinsic semiconductor. There are two kinds of extrinsic semiconductors: n-type and p-type. In n-type semiconductors (Figure 27B) an excess amount of negatively charged electrons is added and these electrons enter the conduction band and allow conduction. In p-type semiconductors (Figure 27C) electrons are removed from the valence band, leaving it with "holes". Since the valence band is no longer full, it has been turned into a conduction band, and electric current can flow.[25] Titanium dioxide is an n-type semiconductor [70]. Upon photoexcitation by light the dye molecules adsorbed in the TiO_2 films inject electrons into the conduction band of the semiconductor film, thus promoting electronic conduction. This is the reason why the LUMO of the dye should be near the conduction band of TiO_2, to ensure electron transfer to the semiconductor (Eq. 2a) instead of decay to the ground state of the dye (Eq. 2b).

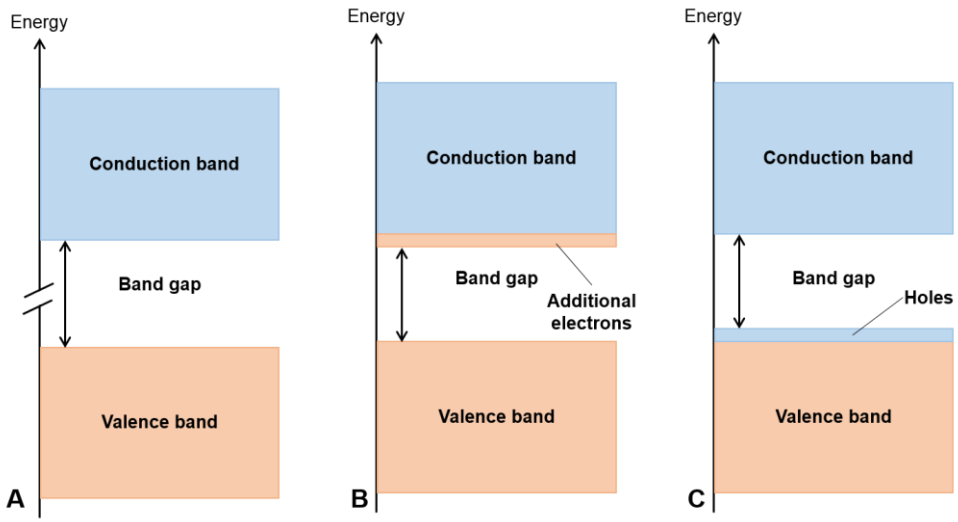

Figure 27. Schematic representation of band energies in three types of substances. **A-** In an insulating solid, a full valence band is separated by a substantial energy gap from the empty conduction band. **B-** In an n-type semiconductor an excess negatively charged electrons enter the conduction band where they can act as current-carriers. **C-** In a p-type semiconductor the removal of electrons from the valence band results in "holes" that enable the remaining electrons to gain mobility and conduct electricity through the valence band.

The sol-gel method of synthesis used to produce the films was the same applied in chapter 2.1 to obtain the TiO_2 powder, but instead of proceeding with the calcination step, the prepared solution was first deposited in FTO conducting glass plates to produce a film with an organized structure (Figure 28).

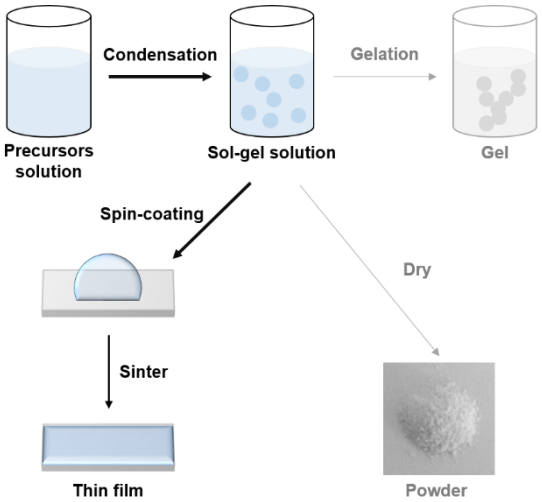

Figure 28. Schematic representation of the TiO_2 thin film synthesis.

A Spray method for the deposition step was applied since it is a simple and innovative technique. This method is based in spraying the solution directly onto the FTO glass slides. Since the spraying device is manually operated, the resulting films depend (and therefore can be manipulated) on the amount of solution sprayed (regulated by an adjustable setting), on the

distance of the spray device to the glass slides, on the number of layers, and on a wide sort of operator differences. Hence the challenge with this technique. Figure 29 shows films obtained by this deposition method. Initially, independently of the number of layers sprayed, all films looked transparent and smooth (Figure 29A). The drawback of this technique revealed to be the low reproducibility. Figure 29B represents films made on the same day, with the same solution and equal number of deposited layers and yet on the second glass there are noticeable imperfections. Even though the glasses were cleaned right before the deposition, and tried to use the same conditions and the same operator, the resulting films revealed inconsistencies between batches of solutions, (using the same solution) between equal number of layers, and so a better alternative was studied.

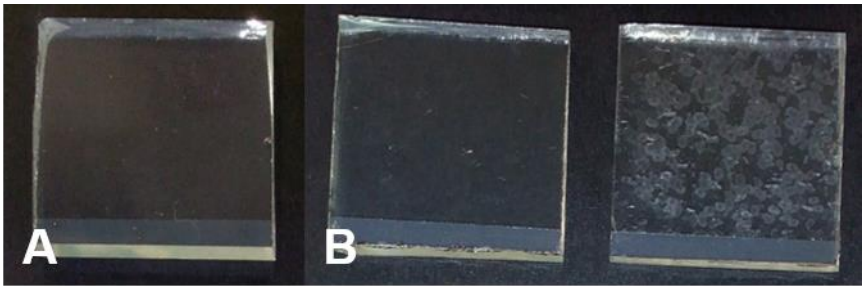

Figure 29. A- Image of the TiO_2 film from spray deposition on top of an FTO conducting glass plate. **B-** Image showing a 5 layer spray deposition TiO_2 film. The one on the left looks normal, the one on the right shows imperfections.

Aiming to guarantee reproducible results, the films were therefore produced using the Spin-coating technique. This method allows the control, with high level of certainty, of settings such as spinning velocity, and therefore to produce replicates with the same layer thickness and characteristics. It is an overall simple and reliable technique that presents reproducible results when working with small areas [43,44].

Producing consistently good films on top of glass slides is usually challenging since it is difficult to guarantee particle deposition and adherence to the glass in a homogenous distribution. To produce an efficient DSSC the semiconductor layer has to be a well-structured, well-organized and highly homogenous film. There are many things that can affect films' homogeneity from dirt and dust, to an inherent lack of affinity of the solution to the glass surface. Glass cleaning previous to solution deposition is of major importance [71]. Lack of affinity is also a serious problem that involves a not so simple solution. To avoid this drawback, a crucial step was added: a "treatment" of the FTO glass slides with a titanium isopropoxide solution. This treatment with titanium isopropoxide will allow the deposition of a small layer of TiO_2 on top of the FTO surface. The purpose was to enhance the affinity of the TiO_2 solution posteriorly deposited, as well as the probability of TiO_2 crystals' formation on top of the glass, therefore avoiding inhomogeneous distribution of the film throughout the glass surface that would result in an inefficient device.

To study the influence of different spin-coating velocities in the final film thickness a range of velocities from [600-1100] rpm was used. Spin-coating technique is based on centrifugal force, therefore the angular velocity of the substrate defines the final film thickness. This means that thinner or thicker films can be produced applying either higher or lower angular velocities, respectively. Since the final application devices needed to take-up charge (e.g. dyes) the use of velocities higher than 1100 rpm was intentionally discarded, thus avoiding the production of ultrathin films. DSSCs' efficiency is directly dependent on light-harvesting by the adsorbed dyes, thus the use of highly porous films. Producing ultrathin films would result in less available surface area for dye adsorption, which would in turn result in less light-harvesting and, consequently, less efficient DSSCs.

SEM and TEM techniques were used to evaluate the films' characteristics. Figure 30 shows the results of the SEM studies. The same amplifications for the films synthesized at 600 (Figure 30A), 800 (Figure 30B) and 1000 (Figure 30C) rpm are presented. An evident high homogeneity and replicability, which is independent of the velocity used, is observed. The films obtained were very homogenous, with a small number of scratches on its surface, as shown in Figure 30.

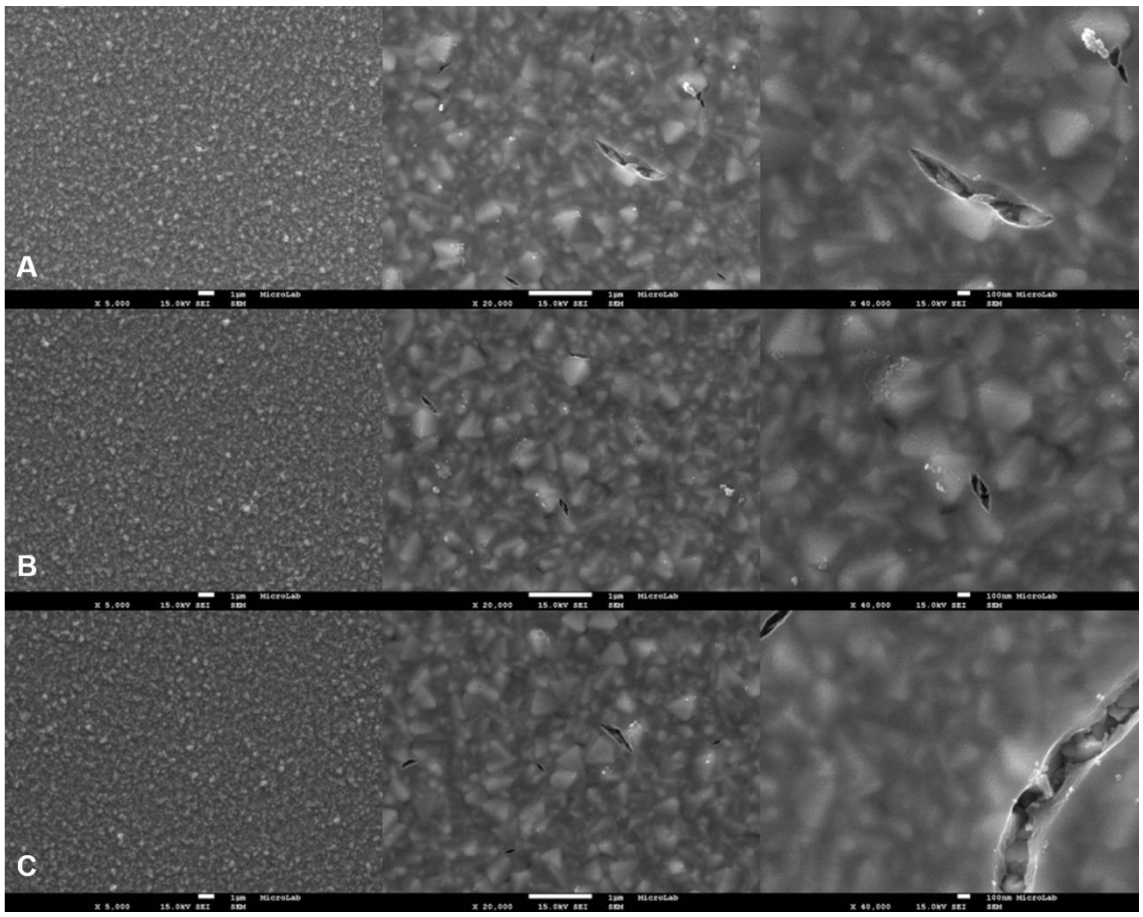

Figure 30. SEM images of the synthesized films. Temperature of calcination: 400ºC. **A-** Film synthesized at 600 rpm. **B-** Film synthesized at 800 rpm. **C-** Film synthesized at 1000 rpm. For each set of velocities three amplifications are presented. From left to right: x5.000, x20.000 and x60.000.

SEM measurements gave the indication that the films produced at 600 rpm have a thickness of about 200 nm. Nonetheless, further measurements, recurring to more suitable measuring techniques, are needed.

Energy-dispersive X-ray spectroscopy (EDS) results of the scratched area confirmed the presence of a TiO_2 film on top of the FTO glass surface (Figure 31).

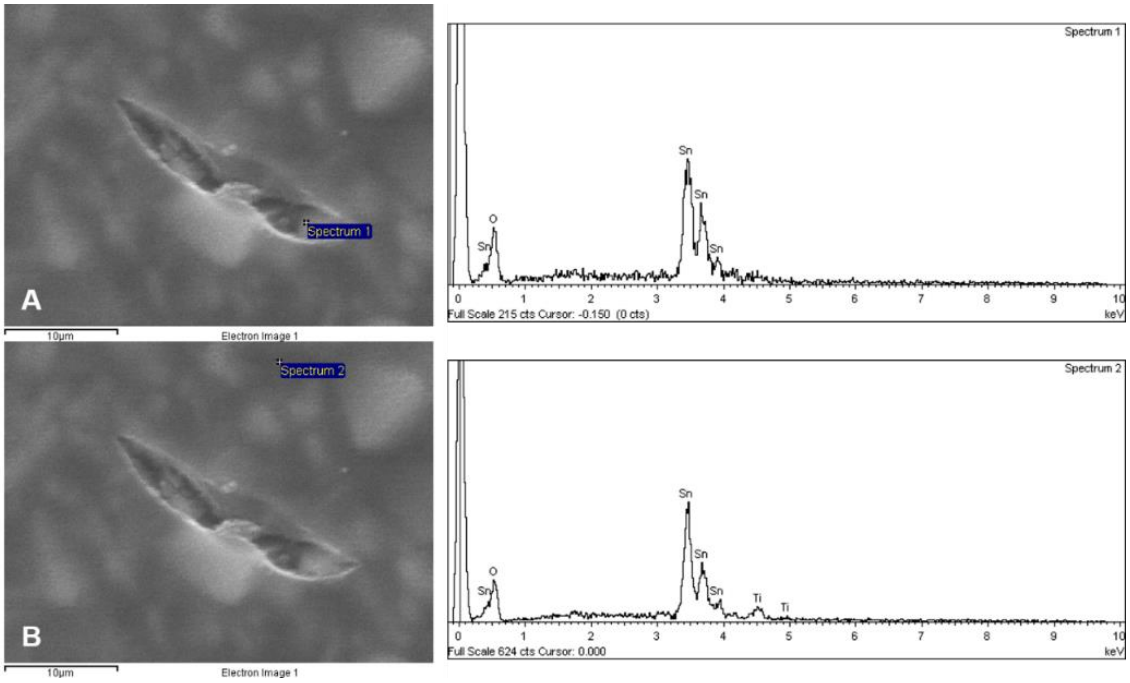

Figure 31. EDS results from the scratched area of the film presented in Figure 30A (Velocity of spin-coating deposition: 600 rpm). **A-** Spectrum 1 is referent to the FTO glass. **B-** Spectrum 2 is referent to the TiO_2 layer.

To evaluate if the films produced were indeed mesoporous, TEM technique was used. In Figure 32A is possible to see the crystalline net of TiO_2, thus proving the presence of a crystalline phase of TiO_2 instead of an amorphous one. This result is quite important, since for the applications intended it is necessary the presence of anatase due to its, already emphasized, unique characteristics. Figures 32B and 32C show pictures of the generalized aspect of the films produced. It is obvious the existence of pores of about 2-3 nm all disposed in an organized manner, resulting in a highly organized mesoporous structure. There is an evident contrast with what was observed in the TEM analysis of the powder, where there was no clear organization, and where well-arranged pores were absent. This analysis proved that one of the main goals of this work was achieved. A highly-organized, mesoscopic TiO_2 film was produced, with a highly porous and homogenous structure, and therefore with a high surface area, which could be used for various applications. These images provided evidence of how promising were the films produced for application in DSSCs. Based in these results we proceeded to the DSSC development.

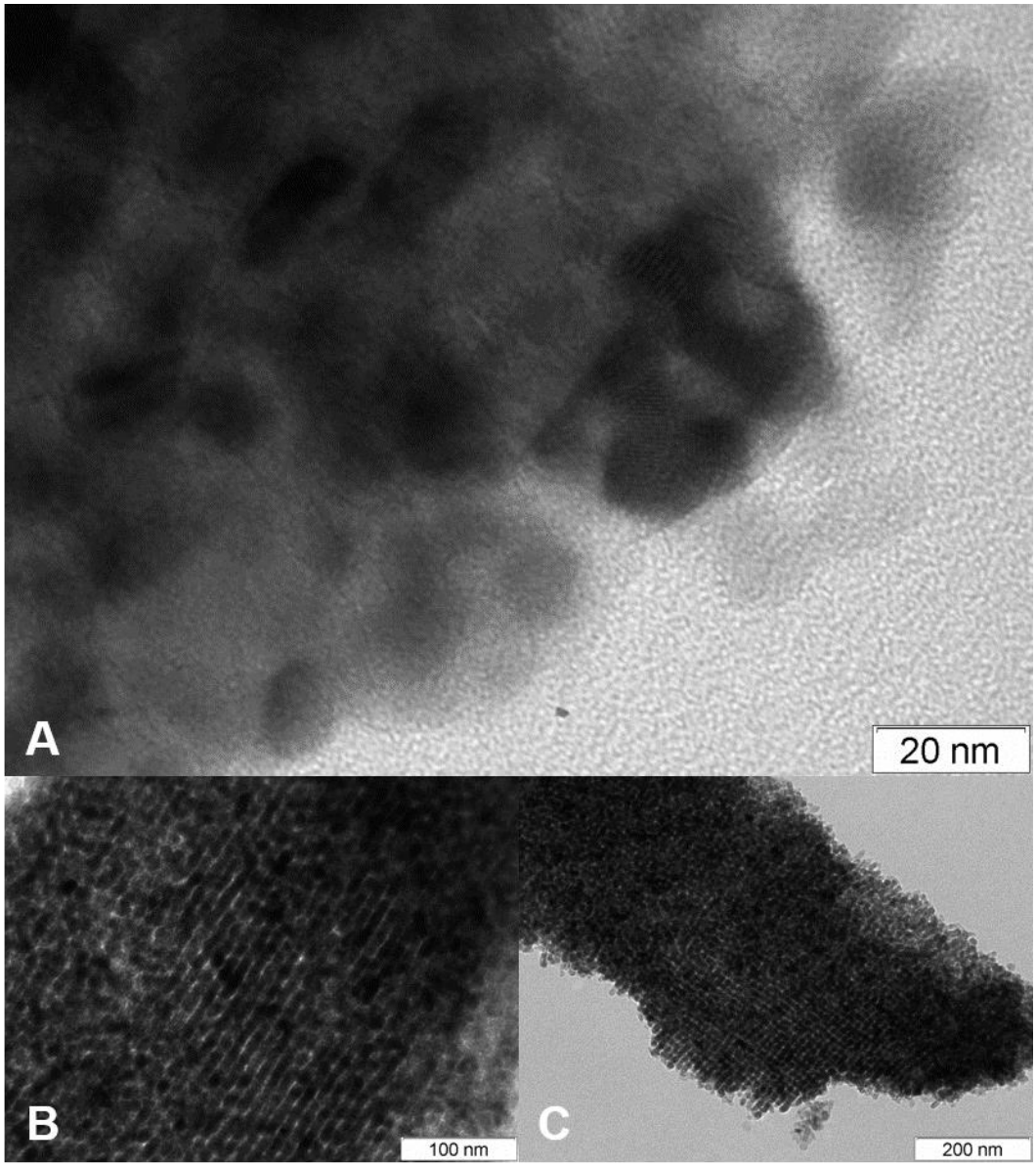

Figure 32. TEM images of the TiO_2 film synthesized at 600 rpm and calcined ate 400ºC.

3.4.1. Dye-Sensitized Solar Cells

Dye-Sensitized Solar Cells (DSSCs), as previously explained, are devices that mimic photosynthesis, which means that they can harvest light and produce energy.

The DSSCs developed in this work were based in the lab procedure suggested in [5] which had already been the inspiration of previous studies developed in the host laboratory [2]. DSSCs based on commercially available anatase (Degussa P25) were produced alongside with the ones based on the synthesized TiO_2 films to serve as comparison.

An important aspect of DSSCs is the presence at all times of an electrolyte with a relay agent, in the case of this work, the I_3^-/I^- redox couple. This electrolyte solution is present in the cell, and penetrates to TiO_2 pores, to assure permanent contact with the adsorbed dye and guarantee its regeneration (Eq. 3a). The electrolyte is then regenerated by electrons from the catalyst (Eq. 4a). This is an example of ionic conduction. If this regenerative agent was not present, a situation similar to that presented in chapter 2.3 would occur. Instead of having a stable system, light harvesting by the dye could promote its photodegradation (depending if the dye itself can be, or not, degraded by this photocatalysis process). Absence of the electrolyte, using an inefficient one or not having it in permanent contact with the dye can compromise the cell's performance. Using a dye with an HOMO that is not sufficiently low in energy for efficient regeneration of its oxidized state by the redox couple can also affect the DSSCs' performance. In this case, instead of promoting the reaction from Eq. 3a, if regeneration is not performed efficiently, the dye can recapture the electrons injected in the TiO_2 conduction band (e^-_{cb}) (Eq. 3b), this way returning to its ground state, resulting in no electronic conduction and, consequently, no electric current production by the cell. Another recombination that would prevent electric current production is the regeneration of the electrolyte by capturing the electrons injected by the dye in the conduction band (e^-_{cb}) of the semiconductor (Eq. 4b). Thus, all the components of a DSSC must be well combined to assure that all the reactions occur in the right time-scale, with no loss of energy through competitive reactions, and promote an efficient working cell.

The DSSCs produced in this work are based in the schematic representation presented in Figure 4. Before building the final DSSC several optimizations had to be performed. The first step was to evaluate the behaviour of prototype cells using commercial anatase (Degussa P25) with different dye sources. This first study was performed with commercial anatase to ensure a means of comparison of the dyes suggested in chapter 2.2 with others reported in [5]. Four dyes were used in this test, the pigment extracted from frozen blueberries [5], and the three dyes studied in chapter 2.2: 3',4',7-trihydroxyflavylium and the pigments extracted from wine and olive oil productions' waste. The TiO_2-coated glass slides were soaked in the dye solutions for approximately 16 hours. Once the glasses were removed from the solutions they had the colour of the dye solution they were placed on, indicating dye adsorption into the TiO_2 film. The TiO_2 layer from the blueberry solution was purple, as well as the one from the wine waste solution, the one from the synthetic flavylium was red, and finally, the one from the olive oil waste was yellow. Table 4 illustrates the results obtained upon approximately 2 minutes of irradiation with an OSRAM 300W solar lamp placed 20 cm above the cells. The results presented were measured using a DP1000 multimeter.

Table 4. Results obtained from the DSSC montage, using commercial TiO_2 (Degussa P25), and different sensitizers. Irradiation performed with a solar lamp placed 20 cm above the cells, for ≈2 minutes.

Sensitizer	V_{oc} (mV)
Blueberry	390
3',4',7-trihydroxyflavylium	399
Wine waste	408
Olive oil waste	350

The results observed (colour adsorption) and present in Table 4 fall within the expected. Pigment adsorption was verified in the TiO_2 powder samples (chapter 2.2) which is in the anatase phase. Since the commercial powder is a mixture of anatase and rutile (3:1), and with overall similar characteristics to the synthesized powder (analysed in chapter 2.1), a similar behaviour was expected. All the dyes in this test possess several =O or –OH groups capable of chelating on the Ti^{4+} sites on the titanium dioxide surface. Furthermore, one of the anthocyanin compounds responsible for blueberry colour, which is proved to adsorb into TiO_2 surface – cyanide-3-glocoside -[5] is also one of the anthocyanins responsible for grape and olive colours. Also the synthetic dye 3',4',7-trihydroxyflavylium had already been used as dye-sensitizer for this commercial TiO_2 (Degussa P25), with an efficiency of 1.22%, resulting from a V_{oc} of 342 mV and J_{sc} of 6.37 $mA.cm^{-2}$ [2]. The V_{oc} values are all similar, with the synthetic and wine waste dyes presenting V_{oc} values slightly higher. Although the potential results are within the predicted (between 300-500 mV [5]) neither of the prepared cells produced measurable electric current, independently of the dye used. These DSSCs should produce a current (J_{sc}) of 1-2 mA/cm^2 for dyed area under bright sunlight [5]. These measurements are not exact since it is a fairly rudimental apparatus and the fact that no current was measured does not imply that these cells cannot produce energy. These results prove, indeed, that the suggested dyes for this study not only can adsorb into the TiO_2 layer, as well as can harvest light and inject electrons into the TiO_2 conduction band, resulting in measurable photovoltage, indicating the potential to electric current production.

Once this study was performed, and concluding that the dyes selected for this work could be used as TiO_2 sensitizers for application in a DSSC, the TiO_2 films synthesized (presented in the beginning of this chapter – chapter 2.4) were used to build novel DSSCs, again based in the schematic representation of Figure 4. We intended to conclude if these synthesized films could function as the semiconductor of a DSSC, and which was the best layer, in terms of the velocities studied.

This study was performed using the synthetic dye as the sensitizer. Using a synthetic dye provides the advantage of controlling the purity and the concentration of the solution. Besides, since this dye was already studied and has reported results [2] it would facilitate the analysis of the produced DSSCs. Layer thickness is also one of the parameters being analysed, since it can affect electron transport through the TiO_2 film into the FTO conductive layer of the glass. To test the semiconductor synthesized and the influence of the film thickness, instead of applying a fixed

time of irradiation as in the previous test, the amount of time necessary for the cell to reach its maximum potential values were also registered. Once again, the glasses were soaked in a 0.5mM ethanol solution of the synthetic flavylium for 16 hours. Table 5 presents the results obtained for the tests performed. Irradiation was performed with an OSRAM 300W solar lamp placed 20 cm above the cells. The results presented were measured using a DP1000 multimeter.

Table 5. Results obtained from the DSSC montage, using 3',4',7-trihydroxyflavylium as the sensitizer, and testing films deposited with different spin-coating velocities and calcined at 400ºC. Irradiation performed with a solar lamp placed 20 cm above the cells.

Semiconductor film	Approximate time of irradiation (min)	V_{oc} (mV)
Commercial Anatase	3	400
TiO_2 film - 600 rpm	1	375
TiO_2 film - 700 rpm	1	364
TiO_2 film - 800 rpm	1	365
TiO_2 film - 900 rpm	1	334
TiO_2 film - 1000 rpm	1	333
TiO_2 film - 1100 rpm	1	335

All the cells with the synthesized TiO_2 film took approximately the same amount of time, ≈1 minute, to reach their maximum potentials, which indicates that layer thickness (for the deposition velocities chosen) does not have much influence in the velocity of electron transport through the system. The cell using commercial anatase however took ≈3 minutes to reach its maximum potential. This makes sense since the commercial anatase film is significantly different from the synthesized ones, with a significantly higher thickness. Degussa P25 anatase is a white powder, and the films produced were, therefore, white and almost opaque. The method of deposition is not the same either. The synthesized films result from the spin-coating deposition of a sol-gel solution. Commercial TiO_2 films were prepared by gradually adding an acetic acid solution to the commercial powder, and grinding until a uniform lump-free white paste was obtained. This paste was then deposited on the FTO glass surface by placing three drops of the prepared paste on top of the glass, and then sliding a glass rod over the plate until a uniformly distributed film was obtained. The final thickness of the so produced film was approximately 40-50 μm [5] opposed to the estimated 200 nm of the films synthesized at 600 rpm. This difference in layer thickness might be affecting the results observed since it would take more time for the electron to travel through the semiconductor layer to the electrode.

Despite the different aspect of the films (from commercial to the synthesized), the differences in the potentials obtained are not that significant. Commercial anatase and the TiO_2 film synthesized at 600 rpm have similar V_{oc} results. This may suggest that even with the difference in layer thickness the synthesized films are competitive. The reason may be concerned with the highly organized and highly porous structure of the synthesized films (Figure 32). Film porosity and

organization greatly enhance the available surface area for dye adsorption. Consequently, in spite of the thin layer, the synthesized films can be promoting greater dye adsorption, and therefore a greater amount of electron injection into the TiO_2 conduction band. A slight decrease from 375 mV for 600 rpm to 335 mV for 1100 rpm (a decrease of 40 mV *per* a 500 rpm increase) is observed, representing a decrease in potential with the decrease of the layer thickness. These results make sense since a thinner layer would probably take up less charge (dye) and consequently affect negatively the cell's behaviour. This indicates that the differences in layer thickness may not affect the time it takes for the cell to achieve its maximum potential, but affects the maximum potential achieved because once we increase the layer thickness, the number of recombination centres are also expected to increase (although this behaviour is not linear) [72]. Again, no measurable current was produced by the devices tested. But the presence of such significant photovoltage values is an indicative of the cells' potential to produce current. Based on the results obtained and due to the arguments presented, the TiO_2 film chosen to proceed the study was the one deposited at 600 rpm.

Once proven the ability of the studied dyes to work as sensitizers for application in DSSCs, and having optimized the semiconductor layer, the final step of this work was to put all the studied and optimized parts together to assemble and test a DSSC. This DSSC was based on the dye-sensitization of a synthesized TiO_2 film by a natural red fruit pigment, in this case from the extraction of dye from wine and/or olive oil productions' waste. Hence, the next logical step was the adsorption of the studied dyes into the synthesized films.

Glass slides with TiO_2 films deposited at 600 rpm and calcined at 400ºC were soaked in the natural dye solutions for approximately 16 hours. After removal from the solution the results observed were not as expected. No dye adsorption had occurred. Figure 33 shows a comparison of the TiO_2 films after soaking in the synthetic dye flavylium (Figure 33A) (from the tests present in Table 4) and after 16 hours soaking in solution with dye prevenient from the wine waste extraction (Figure 33B).

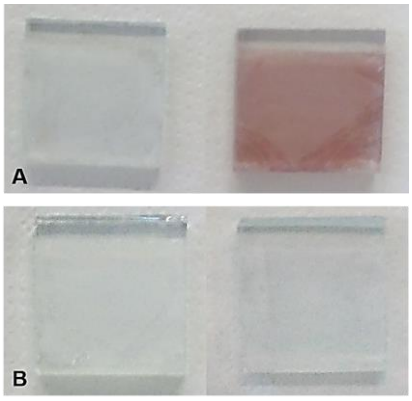

Figure 33. A- Picture of the synthesized TiO_2 film deposited at 600 rpm and calcined at 400ºC before (on the left) and after (on the right) soaking in a $5x10^{-4}$ M 3',4',7-trihydroxyflavylium ethanol solution, pH≈1. **B-** Picture of the synthesized TiO_2 film deposited at 600 rpm and calcined at 400ºC before (on the left) and after (on the right) soaking on the ethanol solution of dye extracted from the wine production's waste, pH≈2.

In Figure 33A there is an evident difference from the film before (on the left) and after soaking in the 3',4',7-trihydroxyflavylium solution (on the right). The film turns from almost transparent to red. In Figure 33B, there is no difference in film colour before (on the left) and after soaking in the solution of dye extracted from the wine waste (on the right). Similar results were obtained with the dye extracted from the olive oil waste. Several approaches were applied to overcome these results. New batches of films were used since this inability to adsorb dye could be due to a defect in the films produced. A sintering process was applied to the films produced: 450ºC for 2 hours, heating ramp of 120ºC/h. Given the presence of organic matter still entrapped in the pores (as discussed in chapter 2.1), dye adsorption could be prevented since the pores were "occupied". Neither of these changes led to the results expected. Another attempt was made, and the films were left soaking in the dye solutions for more than 24 hours. Still, when removing the glasses from the solutions, the films did not adsorb any pigment. Slight pH variations (≈1.0 above and below the previously defined optimal pH) were used in the dye solutions, and still no adsorption was verified. This can be due to the fact that natural anthocyanins have pendant sugars and thus, the molecule is bigger than the synthetic flavylium used to obtain the results from Table 5. The pores of the synthesized film can be too narrow, thus the molecules from the natural dye cannot diffuse to the structure and adsorb into TiO_2. Further pH studies could be developed, changing the pH of the solution from ≈0.1 values, above and below, to see if these changes could influence positively the outcome of the adsorption results.

Efficiency tests were performed to assess about the characteristics of the DSSCs developed. These tests were not carried out in the host laboratory, but in LEPABE – Laboratory for Process Engineering, Environment, Biotechnology and Energy, Faculty of Engineering, University of Porto, by Dr Luisa Andrade and Dr Cláudia Costa.

The efficiency tests aimed to evaluate the photovoltaic performance of the cell. The DSSCs tested used the synthesized TiO_2 films but the dye-sensitizer used was neither of the ones developed by us. The dye used was N719, a ruthenium based dye, which had proved to be one of the most efficient dyes used in DSSCs [73,74]. Table 6 and Figure 34 present the best result obtained with such DSSCs. Table 6 also presents results reported from DSSCs using the dye N719 adsorbed onto a ≈5 µm mesoporous TiO_2 film [75]. The efficiency results obtained were of 0.85% which is low compared with the reported results, where a result of ≈10% was obtained [75]. These efficiency results were calculated based on equation 6. The I_s, V_{oc} and FF results, which are respectively the Incident light intensity, the open circuit photovoltage and the fill factor, present approximately the same values, thus these are not the determining factors affecting this great difference in the efficiency results. The major difference is in the J_{sc} values, the photocurrent produced. The DSSC using the synthesized TiO_2 produced only 1.77 $mA.cm^{-2}$, whereas the reported cell produced a 19.9 $mA.cm^{-2}$ photocurrent. These photocurrent results are the major factors affecting the efficiency. The cells using the synthesized TiO_2 did not produce high photocurrent values. This can be because of inefficient electron injection of the dye into the produced TiO_2, the TiO_2 might be performing an inefficient transport of the electrons into the FTO conductive layer, and so on.

However, the low results verified are probably due to film thickness. As mentioned before the TiO_2 films are predicted to have a layer thickness of about 200 nm, according to the SEM technique. Since the usual layer thickness is in the micrometre scale, this fact can greatly influence the performance of the cell. As explained before, the performance of the cell depends on light harvesting, which in turn depends on the amount of dye adsorbed, consequently, if the film produced is too thin, there is a reduced amount of dye adsorbed and therefore the efficiency results are not as high as expected.

Table 6. Photovoltaic performance of the DSSC with the synthesized TiO_2 film deposited at 600 rpm and calcined at 400ºC, using N719 as dye-sensitizer, from the efficiency tests performed at LEPABE; vs. the results reported for a DSSC using TiO_2 as the semiconductor and N719 sensitization [75].

	Active area of the DSSC (cm^2)	**I_s ($mW.cm^{-2}$)**	**V_{oc} (V)**	**J_{sc} ($mA.cm^{-2}$)**	**P_{max} ($mW.cm^{-2}$)**	**Fill Factor (FF)**	**Efficiency (%)**
DSSC Present work	0.20	92	0.7	1.77	0.78	0.63	0.85
Reported results[75]	-	100	0.8	19.9	-	0.66	10.1

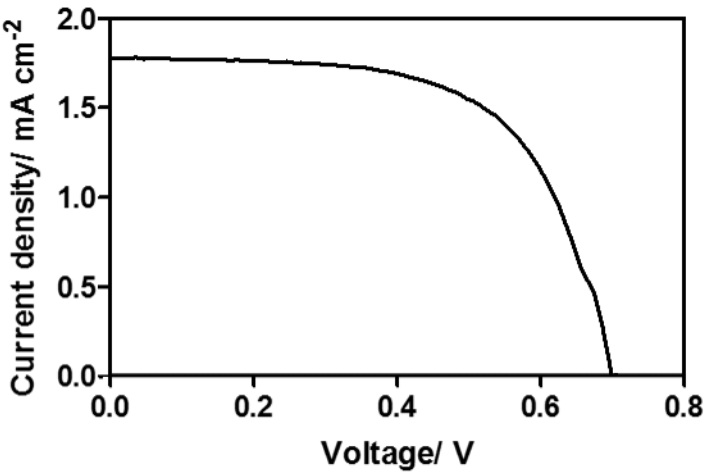

Figure 34. J_{sc} - V curve of the DSSC with the synthesized TiO_2 film deposited at 600 rpm and calcined at 400ºC, using N719 as dye-sensitizer, from the efficiency tests performed at LEPABE.

3.5. Conclusions and Future work

Aiming to produce electrical energy based on the photosynthetic process that occurs in Nature, we intended to develop a dye-sensitized solar cell. Such a device was based on the adsorption of biological compounds (such as naturally occurring anthocyanins) onto titanium dioxide, as a biotechnological application. In these DSSCs anthocyanins were used to perform the light-harvesting role (which in Nature is attributed to chlorophylls), instead of playing their naturally ascribed role. To produce a dye-sensitized solar cell there are several intermediate requirements that need to be satisfied. In this work we developed all the layers of the final DSSC.

The sol-gel strategy followed, allowed the synthesis of mesoporous titanium dioxide powders and films in anatase crystalline phase. Following the nanoparticles' formation by DLS abled the understanding of the TiO_2 nanoparticles' formation and growth. A model was suggested where $Ti(OH)_4$ molecules partition to the micelles and condensate only (or at least mainly) on the micelles' surface to form TiO_2. Pluronic P123 not only serves as a template for the mesoporous structure of TiO_2, but it also works as a sort of catalyst since condensation processes occur predominantly on the micelles surface and not in the solution. DLS studies allowed to determine a single-exponential growth for the TiO_2 nanoparticles, with a final diameter (independent of the temperature of reaction) of about (mean value) 13.4 nm. Further studies could be performed, varying TEOT and/ or Pluronic P123 initial concentrations to better understand what is determining the nanoparticles' final volume. The powders produced were all mesoporous and correspondent to the anatase crystalline phase of titanium dioxide. The powder synthesized and calcined at 400ºC presented largely increased BET surface area and pore volume in comparison with the widely used commercial anatase Degussa P25.

Three different dyes were suggested to sensitize TiO_2: 3',4',7-trihydroxyflavylium, a synthetic analogue of anthocyanins, and the pigments extracted from wine and olive oil productions' waste. pK_a and pK'_a values were calculated for the synthetic dye (pK_a= 3.04 and pK'_a=1.98) and for the pigment extracted from the wine waste (pK_a=3.17 and pK'_a=3.07), concluding that the equilibrium composition is closer to the initial composition than what was observed in the synthetic flavylium. The pigment extracted from the wine waste revealed the presence of anthocyanins, whereas the pigment extraction from the olive waste would have to be optimized using, for example, a different solvent, since no anthocyanin extraction occurred. For both the natural samples HPLC studies would have to be performed to characterize the components extracted from the biological waste. All the dyes adsorbed onto the synthesised TiO_2 powder calcined at 400ºC. Furthermore, the three dyes proved to be good sensitizers for the commercial TiO_2 (Degussa P25) in DSSC application. However only the synthetic dye was successfully adsorbed and used as sensitizer when assembling DSSCs with the synthesized TiO_2 films.

The photodegradation study performed fulfilled the 'proof of concept' purpose. We were able to degrade the pigment from the wine waste adsorbed in the synthesized TiO_2, irradiating the sample in the visible part of the light spectrum. This proved that TiO_2 works as a catalyst to

photodegradation processes, and can be used to degrade contaminant compounds, such as dyes from the textile industry, or, like in this study, from wine and olive oil production. Further studies can be developed to optimize this process and maybe develop a dye that works as an *antennae* but is not degraded itself by TiO_2. This would allow the system to absorb visible light and enhance the catalytic capacity of TiO_2 without the loss of the light harvesting element, and would even facilitate the degradation of colourless compounds.

The TiO_2 films produced were highly homogenous and presented an extremely organized structure. The films presented pores of about 2-3 nm all disposed in an organized manner. Although we were able to adsorb dyes into the TiO_2 layer, we suspect that the layer is too thin, and that affected the overall performance of the DSSCs produced. Increasing the number of layers deposited by spin-coating, or using another deposition technique, such as doctor blading, which allows to control the final film thickness, are options to be explored in order to increase layer thickness and, therefore, enhance the efficiency of the cells produced.

We were not able to fulfil the final objective of constructing a DSSC based on natural pigments from red fruits, such as grape. Although the dye had worked as a sensitizer when adsorbed in commercial anatase (Degussa P25), in the synthesized TiO_2 dye adsorption did not occur. Further studies and optimizations would have to be performed to understand and overcome this drawback.

4. References

1. Alberius, P. C. A., Frindell, K. L., Hayward, R. C., Kramer, E. J., Stucky, G. D. and Chmelka, B. F. General predictive syntheses of cubic, hexagonal, and lamellar silica and titania mesostructured thin films. *Chem. Mater.* **14,** 3284–3294 (2002).

2. Calogero, G., Sinopoli, A., Citro, I., Di Marco, G., Petrov, V., Diniz, A. M., Parola, A. J. & Pina, F. Synthetic analogues of anthocyanins as sensitizers for dye-sensitized solar cells. *Photochem. Photobiol. Sci.* **12,** 883–94 (2013).

3. Crossland, E. J. W., Noel, N., Sivaram, V., Leijtens, T., Alexander-Webber, J. A. & Snaith, H. J. Mesoporous TiO_2 single crystals delivering enhanced mobility and optoelectronic device performance. *Nature* **495,** 215–9 (2013).

4. Velasco, L. F., Fonseca, I. M., Parra, J. B., Lima, J. C. & Ania, C. O. Photochemical behaviour of activated carbons under UV irradiation. *Carbon N. Y.* **50,** 249–258 (2012).

5. Smestad, G. P. Demonstrating Electron Transfer and Nanotechnology : A Natural Dye – Sensitized Nanocrystalline Energy Converter. *J. Chem. Educ.* **75,** 752–756 (1998).

6. Biotechnology Industry Orginization. *Healing, Fueling, Feeding: How Biotechnology Is Enriching Your Life. Biotechnology* (2010).

7. Bar-Cohen, Y. Biomimetics--using nature to inspire human innovation. *Bioinspir. Biomim.* **1,** P1–P12 (2006).

8. Bhushan, B. Biomimetics: lessons from nature--an overview. *Philos. Trans. A. Math. Phys. Eng. Sci.* **367,** 1445–1486 (2009).

9. Sadava, D., Hillis, D. M., Heller, H. C. & Berenbaum, M. R. in *Life: The Science of Biology* 189–208 (Sinauer Associates, 2011).

10. Pina, F., Melo, M. J., Laia, C. A. T., Parola, A. J. & Lima, J. C. Chemistry and applications of flavylium compounds: a handful of colours. *Chem. Soc. Rev.* **41,** 869 (2012).

11. Thirugnanasambandam, M., Iniyan, S. & Goic, R. A review of solar thermal technologies. *Renew. Sustain. Energy Rev.* **14,** 312–322 (2010).

12. Parida, B., Iniyan, S. & Goic, R. A review of solar photovoltaic technologies. *Renew. Sustain. Energy Rev.* **15,** 1625–1636 (2011).

13. Panwar, N. L., Kaushik, S. C. & Kothari, S. Role of renewable energy sources in environmental protection: A review. *Renew. Sustain. Energy Rev.* **15,** 1513–1524 (2011).

14. O'Regan, B. & Grätzel, M. A low-cost, high-efficiency solar cell based on dye-sensitized colloidal TiO2 films. *Nature* **353,** 737–740 (1991).

15. Grätzel, M. Photoelectrochemical cells. *Nature* **414,** 338–344 (2001).

16. Grätzel, M. Solar energy conversion by dye-sensitized photovoltaic cells. *Inorg. Chem.* **44**, 6841–6851 (2005).

17. Grätzel, M. Mesoporous oxide junctions and nanostructured solar cells. *Curr. Opin. Colloid Interface Sci.* **4,** 314–321 (1999).

18. Grätzel, M. Molecular Photovoltaics. *Acc. Chem. Res.* **33,** 269–277 (2000).

19. Hafez, H., Lan, Z., Li, Q. & Wu, J. High efficiency dye-sensitized solar cell based on novel TiO_2 nanorod/nanoparticle bilayer electrode. *Nanotechnol. Sci. Appl.* **3,** 45–51 (2010).

20. Deb, S. K., Ellingson, R., Ferrere, S., Frank, A. J., Gregg, B. A., Nozik, A. J., Park, N. & Schlichthörl, G. Photochemical solar cells based on dye-sensitization of nanocrystalline TiO_2. *AIP Conf. Proc.* 145–153 (1997).

21. Wang, Q., Moser, J. E. & Grätzel, M. Electrochemical impedance spectroscopic analysis of dye-sensitized solar cells. *J. Phys. Chem. B* **109,** 14945–53 (2005).

22. Grätzel, M. Recent Advances ins sensitized Mesoscopic Solar Cells. *Acc. Chem. Res.* **42,** 1788–1798 (2009).

23. Klabunde, K. J., Stark, J., Koper, O., Mohs, C., Park, D. G., Decker, S., Jiang, Y.,Lagadic, I. & Zhang, D. Nanocrystals as stochiometric reagents with unique surface chemistry. *J. Phys. Chem*. **100**, 12142–12153 (1996).

24. in *Springer Handbook of Condensed Matter and Materials Data* (eds. Martienssen, W. & Warlimont, H.) 1031–1072 (Springer-Verlag Berlin Heidelberg, 2005).

25. Atkins, P. & Jones, L. *Chemical Principles: The quest for insight*. (Clancy Marshal, 2010).

26. Hoffmann, M. R., Martin, S. T., Choi, W. &Bahnemannt, D. W. Environmental Applications of Semiconductor Photocatalysis. *Chem. Rev.* **95,** 69–96 (1995).

27. Sekiya, T., Ichimura, K., Igarashi, M. & Kurita, S. Absorption spectra of anatase TiO2 single crystals heat-treated under oxygen atmosphere. *J. Phys. Chem. Solids* **61,** 1237–1242 (2000).

28. Dambournet, D., Belharouak, I. & Amine, K. Tailored preparation methods of TiO2 anatase, rutile, brookite: Mechanism of formation and electrochemical properties. *Chem. Mater.* **22,** 1173–1179 (2010).

29. Marinescu, C., Sofronia, A., Rusti, C., Piticescu, R., Badilita, V., Vasile, E., Baies, R. & Tanasescu, S. DSC investigation of nanocrystalline TiO_2 powder. *J. Therm. Anal. Calorim.* **103,** 49–57 (2011).

30. Mills, A. & Le Hunte, S. An overview of semiconductor photocatalysis. *J. Photochem. Photobiol. A Chem.* **108,** 1–35 (1997).

31. Gao, P., Gratzel, M. & Nazeeruddin, M. K. Organohalide Lead Perovskites for Photovoltaic Applications. *Energy Environ. Sci.* **7,** 2448–2463 (2014).

32. He, M., Zheng, D., Wang, M., Lin, C. & Lin, Z. High efficiency perovskite solar cells: from complex nanostructure to planar heterojunction. *J. Mater. Chem. A* **2,** 5994 (2014).

33. Kazim, S., Nazeeruddin, M. K., Grätzel, M. & Ahmad, S. Perovskite as light harvester: A game changer in photovoltaics. *Angew. Chemie - Int. Ed.* **53,** 2812–2824 (2014).

34. Hagfeldt, A., Boschloo, G., Sun, L., Kloo, L. & Pettersson, H. Dye-Sensitized Solar Cells. *Chem. Rev.* **110**, 6595–6663 (2010).

35. Calogero, G., Di Marco, G., Caramori, S., Cazzanti, S., Argazzi, R. & Bignozzi, C. A. Natural dye senstizers for photoelectrochemical cells. *Energy Environ. Sci.* **2,** 1162 (2009).

36. Calogero, G., Yum, J. H., Sinopoli, A., Di Marco, G., Grätzel, M. & Nazeeruddin, M. K. Anthocyanins and betalains as light-harvesting pigments for dye-sensitized solar cells. *Sol. Energy* **86,** 1563–1575 (2012).

37. Hug, H., Bader, M., Mair, P. & Glatzel, T. Biophotovoltaics: Natural pigments in dye-sensitized solar cells. *Appl. Energy* **115,** 216–225 (2014).

38. Calogero, G., Di Marco, G., Cazzanti, S., Caramori, S., Argazzi, R., Di Carlo, A. & Bignozzi, C. A. Efficient dye-sensitized solar cells using red turnip and purple wild Sicilian prickly pear fruits. *Int. J. Mol. Sci.* **11,** 254–267 (2010).

39. Zhou, H., Wu, L., Gao, Y. & Ma, T. Dye-sensitized solar cells using 20 natural dyes as sensitizers. *J. Photochem. Photobiol. A Chem.* **219,** 188–194 (2011).

40. Calogero, G., Bartolotta, A., Di Marco, G., Di Carlo, A. & Bonaccorso, F. Vegetable-based dye-sensitized solar cells. *Chem. Soc. Rev.* (2015).

41. Brouillard, R. in *The Flavonoids* (ed. Harborne, J. B.) 525–538 (Springer US, 1988).

42. Bridle, P. & Timberlake, C. F. Anthocyanins as natural food colours—selected aspects. *Food Chem.* **58,** 103–109 (1997).

43. Krebs, F. C. Fabrication and processing of polymer solar cells: A review of printing and coating techniques. *Sol. Energy Mater. Sol. Cells* **93,** 394–412 (2009).

44. Aegerter, M. A. & Mennig, M. in *Sol-Gel Technologies for Glass Producers and Users* 49–55 (Kluwer Academic Publishers, 2004).

45. Santos, C. M., Gomes, B., Gonçalves, L. M., Oliveira, J., Rocha, S., Coelho, M., Rodrigues, J. A., Freitas, V. & Aguilar, H. Pyranoflavylium Derivatives Extracted from Wine Grape as Photosensitizers in Solar Cells. *J. Braz. Chem. Soc.* **25,** 1029–1035 (2014).

46. Orak, H. H. Total antioxidant activities, phenolics, anthocyanins, polyphenoloxidase activities of selected red grape cultivars and their correlations. *Sci. Hortic. (Amsterdam).* **111,** 235–241 (2007).

47. Piga, A., Del Caro, A., Pinna, I. & Agabbio, M. Anthocyanin and colour evolution in naturally black table olives during anaerobic processing. *LWT - Food Sci. Technol.* **38,** 425–429 (2005).

48. Aparicio, R. & Harwood, J. *Handbook of Olive Oil*. *Handbook of Olive Oil* (2013).

49. Vinha, A. F., Ferreres, F., Silva, B. M., Valentão, P., Gonçalves, A., Pereira, J. A., Oliveira, M. B., Seabra, R. M. & Andrade, P. B. Phenolic profiles of Portuguese olive fruits (Olea europaea L.): Influences of cultivar and geographical origin. *Food Chem.* **89,** 561–568 (2005).

50. Apolo, C. S. & Farma, F. De. Table Olives from Portugal : Phenolic Compounds , Antioxidant Potential , and Antimicrobial Activity. (2006).

51. Romero, C., Garcia, P., Brenes, M., García, A. & Garrido, A. Phenolic compounds in natural black Spanish olive varieties. *Eur. Food Res. Technol.* **215,** 489–496 (2002).

52. Cazoir, D., Fine, L., Ferronato, C. & Chovelon, J. M. Hydrocarbon removal from bilgewater by a combination of air-stripping and photocatalysis. *J. Hazard. Mater.* **235-236,** 159–168 (2012).

53. Minabe, T., Tryk, D. A., Sawunyama, P., Kikuchi, Y., Hashimoto, K. & Fujishima, A. TiO_2-mediated photodegradation of liquid and solid organic compounds. *J. Photochem. Photobiol. A Chem.* **137,** 53–62 (2000).

54. De Mendonça, V. R., Lopes, O. F., Fregonesi, R. P., Giraldi, T. R. & Ribeiro, C. TiO_2-SnO_2 heterostructures applied to dye photodegradation: The relationship between variables of synthesis and photocatalytic performance. *Appl. Surf. Sci.* **298,** 182–191 (2014).

55. Chen, C., Ma, W. & Zhao, J. Semiconductor-mediated photodegradation of pollutants under visible-light irradiation. *Chem. Soc. Rev.* **39,** 4206–4219 (2010).

56. Ferrari-Lima, A. M., Souza, R. P. de, Mendes, S. S., Marques, R. G., Gimenes, M. L. & Fernandes Machado, N. R. C. Photodegradation of benzene, toluene and xylenes under visible light applying N-doped mixed TiO_2 and ZnO catalysts. *Catal. Today* **241,** 40–46 (2015).

57. Li, F. B. & Li, X. Z. The enhancement of photodegradation efficiency using Pt-TiO_2 catalyst. *Chemosphere* **48,** 1103–1111 (2002).

58. Malagutti, A. R., Mourão, H. A. J. L., Garbin, J. R. & Ribeiro, C. Deposition of TiO_2 and Ag:TiO_2 thin films by the polymeric precursor method and their application in the photodegradation of textile dyes. *Appl. Catal. B Environ.* **90,** 205–212 (2009).

59. Inturi, S. N. R., Boningari, T., Suidan, M. & Smirniotis, P. G. Visible-light-induced photodegradation of gas phase acetonitrile using aerosol-made transition metal (V, Cr, Fe, Co, Mn, Mo, Ni, Cu, Y, Ce, and Zr) doped TiO_2. *Appl. Catal. B Environ.* **144,** 333–342 (2014).

60. Zhang, F., Zhaoa, J., Shen, T., Hidakab, H., Pelizzettic, E. & Serponed, N. TiO_2-assisted photodegradation of dye pollutants II. Adsorption and degradation kinetics of eosin in TiO_2 dispersions under visible light irradiation. *Appl. Catal. B Environ.* **15,** 147–156 (1998).

61. Galacho, C., Ribeiro Carrott, M. M. L. & Carrott, P. J. M. Structural and catalytic properties of Ti-MCM-41 synthesised at room temperature up to high Ti content. *Microporous Mesoporous Mater.* **100,** 312–321 (2007).

62. Berne, B. J. & Pecora, R. *Dynamic Light Scattering: With Applications to Chemistry, Biology and Physics*. (Courier Corporations, 1976).

63. Ohno, T., Sarukawa, K., Tokieda, K. & Matsumura, M. Morphology of a TiO_2 Photocatalyst (Degussa, P-25) Consisting of Anatase and Rutile Crystalline Phases. *J. Catal.* **203,** 82–86 (2001).

64. Holzwarth, U. & Gibson, N. The Scherrer equation versus the 'Debye-Scherrer equation'. *Nat. Nanotechnol.* **6,** 534 (2011).

65. Wang, Y.-Q., Chen, S.-G., Tang, X.-H., Palchik, O., Zaban, A., Koltypin, Y. & Gedanken, A. Mesoporous titanium dioxide: sonochemical synthesis and application in dye-sensitized solar cells. *J. Mater. Chem.* **11,** 521–526 (2001).

66. Caputo, A. C., Scacchia, F. & Pelagagge, P. M. Disposal of by-products in olive oil industry: Waste-to-energy solutions. *Appl. Therm. Eng.* **23,** 197–214 (2003).

67. Basílio, N., Fernandes, A., de Freitas, V., Gago, S. & Pina, F. Effect of β-cyclodextrin on the chemistry of 3′,4′,7-trihydroxyflavylium. *New J. Chem.* **37,** 3166 (2013).

68. Basílio, N. & Pina, F. Flavylium network of chemical reactions in confined media: Modulation of 3',4',7-Trihydroxyflavilium reactions by host-guest interactions with Cucurbit[7]uril. *ChemPhysChem* **15,** 2295–2302 (2014).

69. Diniz, A. M., Pinheiro, C., Petrov, V., Parola, a. J. & Pina, F. Synthesis and characterization of a symmetric bis(7-hydroxyflavylium) containing a methyl viologen bridge. *Chem. - A Eur. J.* **17,** 6359–6368 (2011).

70. Nowotny, M. K., Bogdanoff, P., Dittrich, T., Fiechter, S., Fujishima, A. & Tributsch, H. Observations of p-type semiconductivity in titanium dioxide at room temperature. *Mater. Lett.* **64,** 928–930 (2010).

71. Aegerter, M. A. & Mennig, M. *Sol-Gel Technologies for Glass Producers and Users*. (Kluwer Academic Publishers, 2004).

72. Hou, K., Tian, B., Li, F., Bian, Z., Zhao, D. & Huang, C. Highly crystallized mesoporous TiO_2 films and their applications in dye sensitized solar cells. *J. Mater. Chem.* **15,** 2414 (2005).

73. Jin, Z., Masuda, H., Yamanaka, N., Minami, M., Nakamura, T. and Nishikitami, Y. Efficient electron transfer ruthenium sensitizers for dye-sensitized solar cells. *J. Phys. Chem. C* **113,** 2618–2623 (2009).

74. Ryan, M. Progress in ruthenium complexes for dye sensitised solar cells. *Platin. Met. Rev.* **53,** 216–218 (2009).

75. Hwang, S., Lee, J. H., Park, C., Lee, H., Kim, C., Park, C., Lee, M.-H., Lee, W., Park, J., Kim, K., Park, N.-G. & Kim, C. A highly efficient organic sensitizer for dye-sensitized solar cells. *Chem. Commun.* **4887** (2007).